Vibration Excitation of Aerospace Composite Materials for Defect determination using optical NDT techniques (ESPI/Shearography)

AUTHOR : Leovigildo Mahon Gerona

SUPERVISOR : Prof J.Gryzagoridis and D. Findeis

DATE : 31 August 2010

MEC5010Z : MSc. Mechanical Eng. Part Dissertation

Abstract:

This project investigates the detection of structural damage in aerospace composite materials using ESPI and/or Shearography. ESPI and shearography are both laser based digital interferometric techniques used to non-destructively identify defects in small and large structures. Vibration excitation is proposed to be used as the excitation method for the above Non-Destructive Testing (NDT) techniques. The material may or may not contain any defects, in which case the flaws are to be artificially induced.

DECLARATION

1. I know that plagiarism is wrong. Plagiarism is to use another person's work as your own.
2. I have used the Harvard convention for citation and referencing. Each significant contribution to, and quotation in, this project from the work(s) of other peoples has been attributed, cited and referenced.
3. This project is my own work.
4. I have not allowed, and will not allow anyone to copy my work with the intention of passing it off as his/her own work.

Signatureé é

August 2010

ACKNOWLEDGEMENTS

I would like to convey my sincere gratitude first and foremost to God almighty, for empowering me with the knowledge and all the blessings alongside; without whom none of this would have been possible.

I would also like to thank my parents, Mr. Inocencio Mahon and Mrs. Milagrosa Gerona, for their love and support in all my endeavors and for being such wonderful parents to me.

Special thanks to my supervisors, Prof. J. Gryzagoridis and Mr. D. Findeis, for giving me the opportunity to pursuit my masters degree and for guiding me all the way through.

My recognition also to the UCT Mechanical Engineering workshop staff, in particular to Mr. Glen Newins for their contribution in preparing the specimens used for the project.

A special thanks to my girlfriend, Miss. Funeka Zaiyah Qwaka for her love, support and encouragement through the ups and downs in the course of this project.

Finally to all my friends and colleagues that in one way or another have influenced me positively or motivated me to reach the finish line.

Dedication to my parents

Inocencio Mahon Mum and Milagrosa Gerona Alabau

Thank you for all the love and support

TABLE OF CONTENTS

LIST OF FIGURES

LIST OF TABLES

EXECUTIVE SUMMARY

The work presented in this thesis documents an experimental investigation regarding the feasibility of using vibration to excite the energy level of engineering composite materials, when they are being tested non-destructively for defects and flaws.

The investigation was based on the premise that the edges of defects or flaws of the delamination and debonding nature that may have been created during the manufacturing stage or developed during service, would rub together when the component is vibrated. This frictional movement would create localized heating which would affect the surface dimensions of the component.

The Non-Destructive Testing (NDT) methods chosen to attempt the detection of the defects within the body of a composite material component were ESPI (Electronic Speckle Pattern Interferometry) and DS (Digital Shearography). These methods were chosen because they have a history of successful investigation of defect detection in composite structures. These techniques are laser based optical full field non-contacting interferometric methods with proven reliability and excellent sensitivity.

Previous work described in the literature indicates that the preferred mode of specimen/component excitation when using these optical methods has been mild heating for short duration by means of heat lamps or hot air from a hair dryer.

The investigation focused on the detection of defects in aerospace fiber reinforced composite materials (FRCs) and Polycarbonate. Although the choice of components made of composite materials would be relatively incompatible with vibration excitation because of the material possessing ñysteresisò and vibration damping characteristics, the project proceeded aiming at establishing the extent of vibration applicability.

The results as presented using vibration excitation and compared with the results using thermal excitation suggest that the former mode of excitation is severely handicapped by the materialsôproperties mentioned above. The findings are that vibration excitation in FRCs and Polycarbonate for defect determination using ESPI and DS is not recommended.

INTRODUCTION

For many years, aircraft designers have been working to improve the efficiency of aircraft. This is a major concern today for both the commercial and military aircraft as the economy hinders and the price of fuel increases. Knowing that the efficiency of an aircraft depends upon the structural mass, the solution was to use structural materials that are light enough but still provide high strength and stiffness. The aircraft designers could propose theoretical designs that they could not build because the materials needed to construct them did not exist. The quest for such materials introduced the composite materials to the aerospace industry.

Composites are the most important materials to be adapted for aviation since the use of aluminum in the 1920s. The use of composites in aircraft construction can be dated to World War II aircraft when soft fiberglass insulation was used in B-29 fuselages. By the late 1950s, European high performance sailplane manufacturers were using fiberglass as primary structures. By 2005, over 35 percent of new aircraft were constructed of composite materials [1].

The technology on composite materials is rapidly advancing in the aerospace industry. According to Airbus, ñcomposite aircraft components manufactured from carbon-resin ópolasticômaterials are here to stay because world energy supply is in decay; the era of ócheap oilô has ended. The aviation industry has no choice but to continue the development of lighter and more fuel efficient aircraft; a new business model towards nonprofit status is not an optionò [2]. With this regard, the Airbus A350 XWB will come into service with 52% of its structural frame made of composite material (see Fig. 1).

Figure 1: Airbus A350 XWB - Intelligent Airframe / Airbus 2006 [2]

Another large aircraft manufacturer with high ambition in the use of composite materials is Boeing. Boeing has begun assembly on the third flight-test airplane for the 787 Dreamliner. A total of 857 Dreamliners have been ordered since the plane was announced in 2003, making it the fastest-selling wide body airliner in history. The Dreamliner is the first aircraft to be 80% composite by volume, making it lighter and more efficient than competitors [3].

Figure 2: Boeing 787 Dreamliner [3]

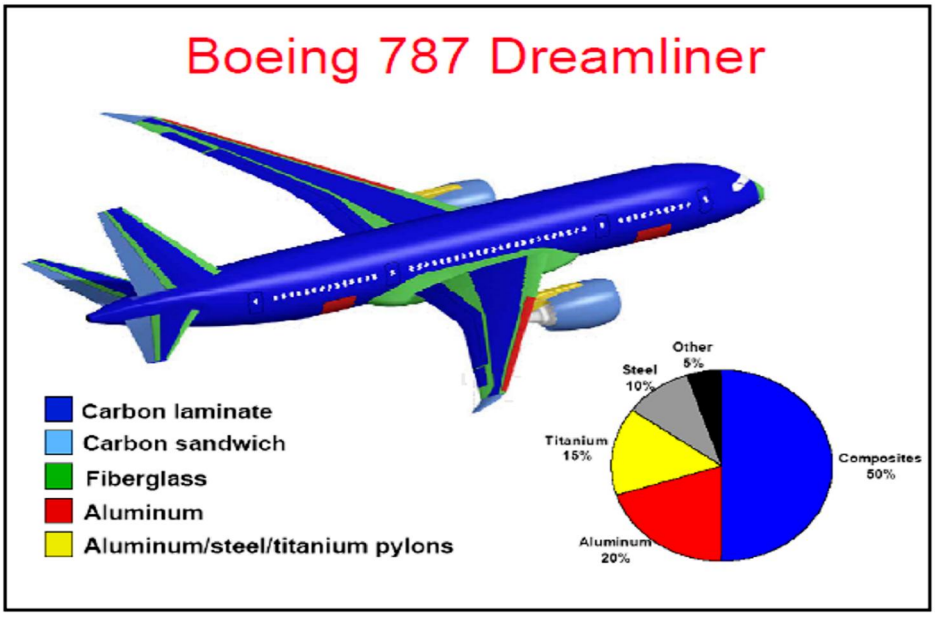

Figure 3: Boeing 787 Dreamliner % Composite [3]

As it can be seen from the figures above, these big giants in the airplane manufacturing industry are not just taking advantage of the higher strength to weight ratio of composites but also because it allows for complex curves and shapes that simply cannot be achieved with comparable aluminum alloys.

Composites have proven to be the material of choice for the future in the aerospace industry because of the benefits presented above, but still, precautions need to be taken so that the widespread use of composites does not compromise aircraft structural integrity. Review of aircraft failure incidents for the past 15 years have put composites in the spotlight and enforced further inspections during manufacturing, testing, and subsequent maintenance.

The problem facing the airline industry today with the use of composites is that they are hard to inspect for flaws. In the aviation industry, these flaws can be as a result of: impact damage, moisture pick-up, lightening strikes or extreme temperatures; if these flaws are detected early enough, major catastrophic events can be prevented.

Many Non-destructive testing (NDT) techniques have been developed for the inspection of composites. Some of these techniques could only detect the relatively large size defect and only limited to the region covered by the transducer. This type of point testing techniques can be time consuming, especially when inspecting a large structure such as an airplane wing or fuselage. The most promising optical techniques that meet the required specifications and are commercially available as fully engineered systems are [4]:

- laser ultrasonic
- transient thermography
- laser shearography and ESPI

In this study only two of the above techniques will be considered, laser shearography and ESPI. To detect flaws using laser shearography or ESPI, energy interaction of one kind or another needs to take place to excite the material in order to give information about the state of the material. Many techniques have been used for this purpose but so far heating has been the preferred method of energy input to excite the test material for

laser shearography/ESPI inspection because of the homogeneity of the input energy distribution and short testing time.

This project is a feasibility study to determine the relevance of using vibration as an alternative excitation technique to expose flaws in aerospace composites under testing with laser Shearography or ESPI. Vibration excitation has been used in analysing structural vibration modes to check for the integrity of materials but no real body of evidence has been presented in the relevant literature of the use of vibration as an excitation technique for optical laser based techniques such as ESPI and Shearograpy, in the detection of flaws and defects. In this respect there is an element of novelty in this study.

CHAPTER 1: LITERATURE REVIEW

Shearographic inspection of aerospace composites has been recognized as a fast and reliable non-destructive inspection technique after many years of phase evaluation. Very similar to shearography is the Electronic Speckle Pattern Interferometry (ESPI) technique which is also an accepted technique for the testing of composites. Researchers at the NDT laboratory of the Mechanical Engineering Department at the University of Cape Town, with over 30 years experience in this field, aim at investigating and perfecting the use of these techniques as it is applied to the relevant industry.

1.1 *Composite Materials for Aerospace Applications*

According to the percentage of composites we have seen being used in aerospace applications today, it is clear that composites are the future of the aerospace industry. Composites are materials that are combinations of two or more organic or inorganic components. One material serves as a ñmatrix,ò while the other material serves as reinforcement, in the form of fibers embedded in the matrix. Until recently, the most common matrix materials were ñthermosettingò, such as epoxy, bismaleimide, or polyimide. The reinforcing materials can be glass fiber, boron fiber, carbon fiber, or other more exotic mixtures [4]. Fig. 4 is the classification of composites according to the reinforcement used.

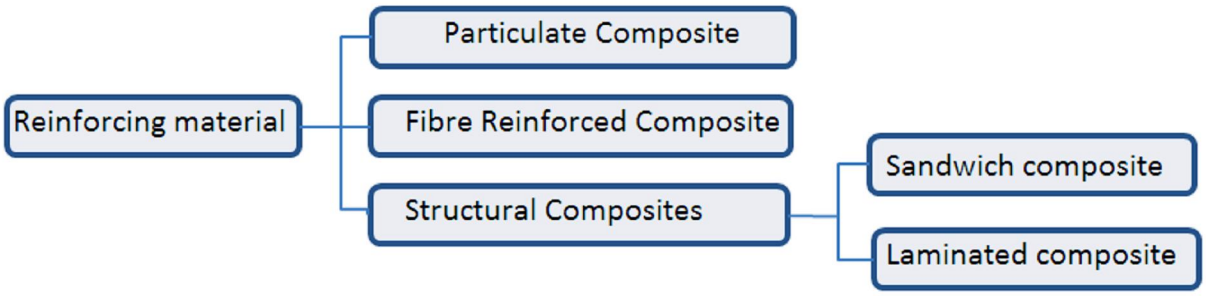

Figure 4: Classification of composite materials according to the reinforcement used [5]

One major concern when combining two materials at microscopic level such as particulate and fibre reinforced composites is the reactivity between the matrix and the reinforcement, as it can influence the final properties of the composite. Reaction between the reinforcement and the matrix can also result in changes in the matrix alloy metallurgy, which in turn influence such basic properties as the melting point of the alloy and its strength [6].

The fiber-matrix combination, also known as ñPrimary Composite Materialsò, reduces the potential for a complete fracture. The rigid fibers impart structural strength to the composite, while the matrix protects the fibers from environmental stress and physical damage and imparts thermal stability to them. Moreover, composites that are made of primary composite materials are determined ñSecondary Composite Materialsò (i.e. sandwich panels composed of composite skins bonded to various core materials such as honeycombs) [7].

While the constituent materials of a composite will determine its mechanical properties, of more commercial importance is how the elementary materials contribute to the increase of the elastic modulus, and this is determined by the rule of mixture expression:

$$E_c = E_m V_m + E_f V_f \qquad Equation\ 1$$

For particulate composite the above equation will be expressed as:

$$E_c = E_m V_m + E_p V_p \qquad Equation\ 2$$

$V_m = {}^{A_m}/_{A_c}$ And $V_f = {}^{A_f}/_{A_c}$ if the fiber and matrix lengths are all equal

Also $V_m + V_f = 1$ since the composite consists of only matrix and fiber

Where E, A and V denote the elastic modulus, area and volume fraction respectively and subscripts *c, m, p* and *f* represent composite, matrix, particle and fiber.

1.1.1 Particulate Composites

Particle-reinforced composites are candidate materials for a wide variety of applications in the aerospace industry. This type of reinforced composite is preferred where shock or impact properties are important [8]; because Particulate composites, just as conventional metallic materials are isotropic, i.e. their properties (strength, stiffness, etc.) are the same in all directions. Some common particulate composites in the aerospace industry are:

- ***Metal matrix composites (MMC);*** usually consist of non-metallic particles in a metallic matrix; for instance silicon carbide particles combined with aluminium alloy. MMCs possess high-temperature capability, high thermal conductivity, low coefficient of thermal expansion, and high specific stiffness and strength. An example of the uses of MMCs in the aerospace industry is graphite/epoxy (Gr/Ep) which has been used in spaceships for truss elements, bus panels, antennas, wave guides, and parabolic reflectors in the past 30 years [9].

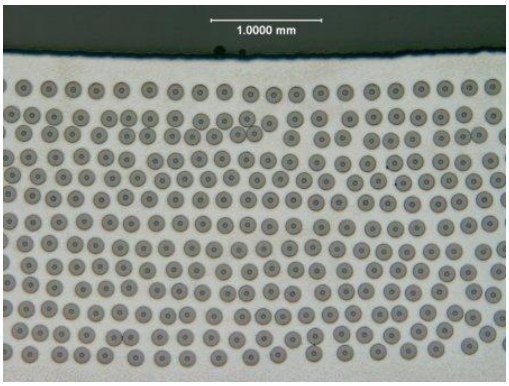

a) **Silicon Carbide fibers in Titanium matrix composite**

b) **Metal Matrix composite with fiber reinforcement**

Figure 5: Metal Matrix Composites [10]

- ***Polimer Matrix Composite (PMC);*** a major drawback of PMCs is poor abrasion resistance, which restricts their use, especially at high temperatures. PMC parts in current aero-engines include fan blades, outlet guide vanes, bypass ducts, nose cone spinners, core engine fairings, annulus fillers and variable guide vane rings [11].

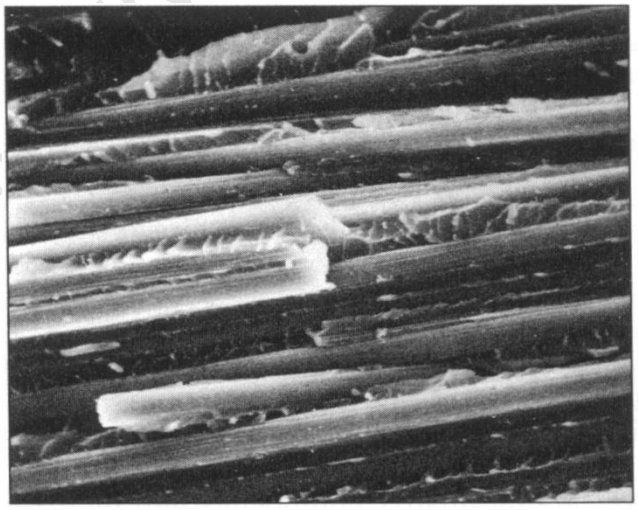

Figure 6: Cross section of carbon fibre embedded in epoxy matrix composite [12]

- ***Ceramic Matrix Composite (CMC);*** were developed originally for limited-life structures in aerospace industry as a lightweight and heat-resistant alternative to metal-based materials. An example of CMCs in common use in aerospace is carbon fiber reinforced silicon carbide (C/SiC) [13].

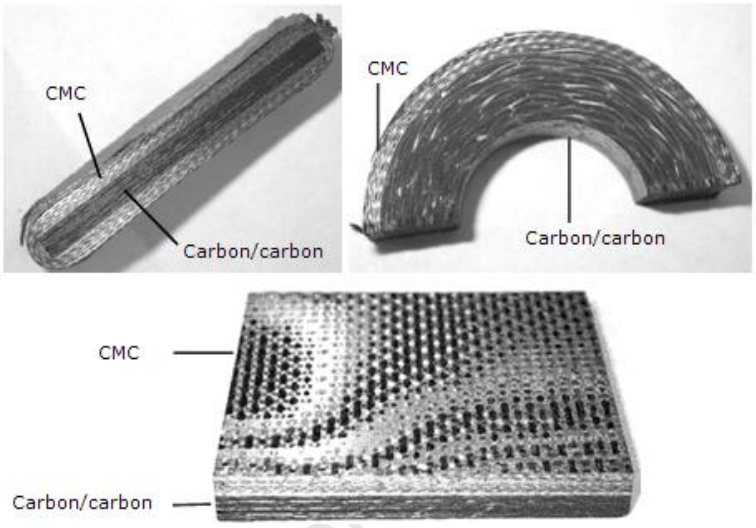

Figure 7: CMC- encased carbon/carbon structures [14]

1.1.2 Fiber Reinforced Composites

These are composite materials which consist of embedded continuous or discontinuous fibers in a matrix material. Fibrous composites are anisotropic, i.e. their properties vary depending on the direction of the load with respect to the orientation of the fibers [15].

Most common fiber-reinforced composites used in aerospace industry are:

- ***Carbon Fiber Reinforced Plastic (CFRP);*** are distinguished by their extremely high strength and rigidity, low density, excellent damping properties and a high resistance to

impacting combined with exactly modifiable thermal expansion to complement the complex characteristics profile. The plastic reinforcement is most often epoxy (as used in the Boeing 787 Dreamliner horizontal and vertical stabilizers), but other plastics, such as polyester, vinylester or nylon, are also used [16].

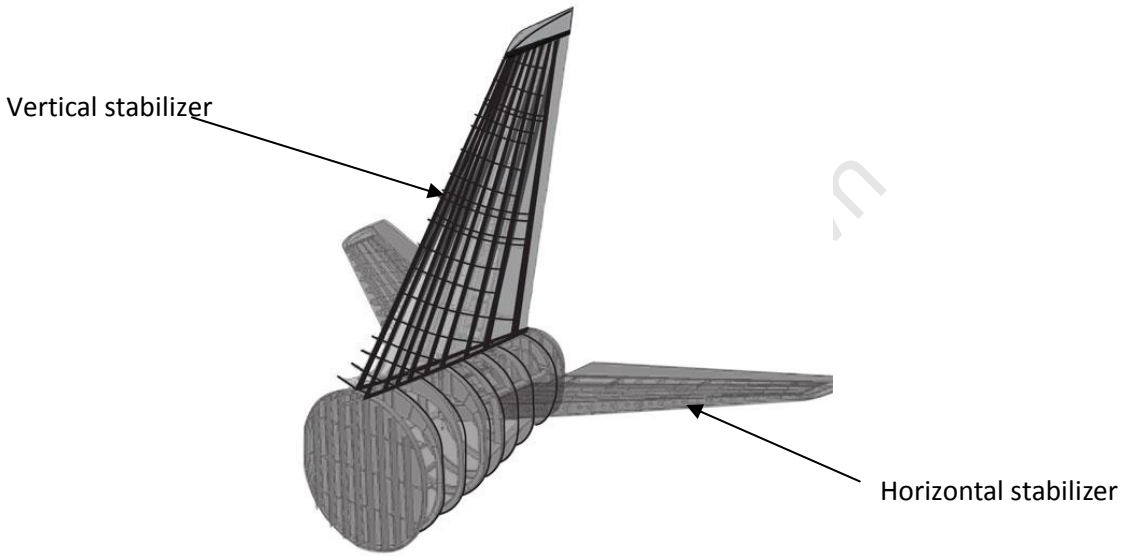

Figure 8: Boein 787 Dreamliner horizontal and vertical stabilizer made of CFRP [34]

- ***Glass Fiber Reinforced Plastic (GFRP);*** are more economically viable than CFRP. This is the reason why they are used in a wide range of applications outside the aerospace industry. GFRPs are used extensively in aerospace industry as a structural insulating material and also in the manufacturing of components such as: wings, nosecones, helicopter rotors, etc.

1.1.3 Structural Composites

- ***Solid Laminates;*** these are composite materials made up of a single ply or layers or a series of layers with each layer consisting of a Reinforcing fiber imbedded in a matrix. Each layer is oriented in a predetermined manner in order to maximize the properties of the laminate [5]. The largest proportion of carbon fiber composites used in primary structures in the aerospace industry (e.g.: wing and fuselage) is fabricated by placing layer upon layer of unidirectional material to designerâs requirement in terms of ply profile and fiber orientation.

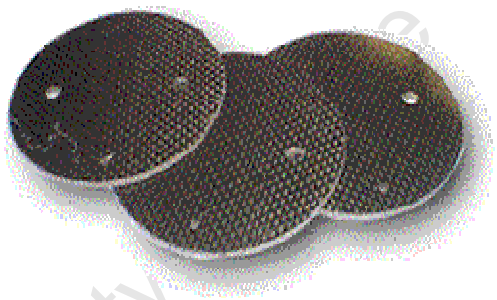

Figure 9: Solid laminate prepreg sheets [17]

- ***Bonded Sandwich Structures;*** a significant benefit of sandwich structures is the fact that they are extremely light while having a high flexural rigidity due to the separation of the surface skins.

  The most extensively used sandwich structure found in the aerospace technology is the honeycomb core sandwich. Usually, this structure includes a core of aluminum or titanium conforming to a honeycomb cell generatrix disposed between rigid face sheets. Honeycomb structures sometimes fail to meet existing needs because the line-contact bonding, established between the honeycomb cell cross section and the face

sheets, can and frequently does lose bonding integrity. In the case of metals, this can be as a result of corrosion [18].

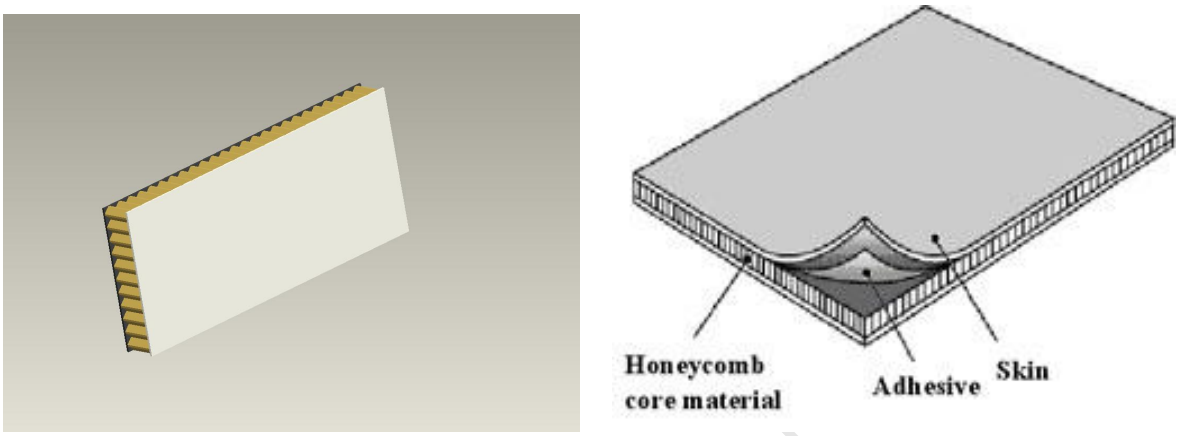

Figure 10: Nomex honeycomb sandwich composite

The composite materials reviewed above are used collectively in the manufacturing of parts in the aerospace industry. An example is the helicopter rotor blade (fig.11) below. Each composite is placed where its mechanical properties are best utilized.

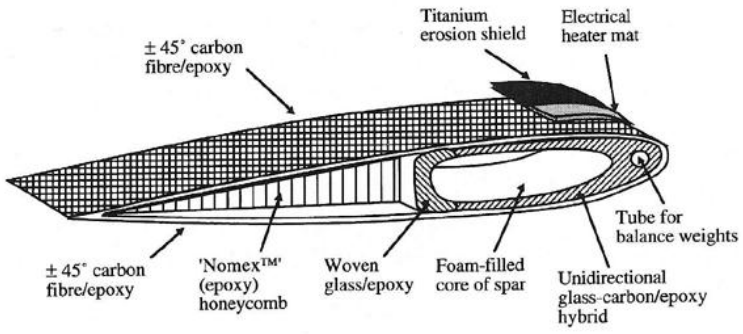

Figure 11: Schematic section through a typical composite construction for a helicopter rotor blade [19]

1.2 *Effect of Composite Bonding in Aerospace applications*

Composite materials can be assembled in a structure either by mechanical fixtures, adhesive bonding or by using inserts. Adhesive bonding has been very promising, especially in the manufacturing of honeycomb structures. It has also presented a number of advantages such as: reduction of parts in a component, eliminate the need of drilling holes, exhibit lower stress concentration at the joints, etc.

Likewise, adhesive bonding has its disadvantages which compromise their use in certain applications. Some of the disadvantages are: poor creep resistance at elevated temperatures (this means that adhesives cannot be used in or near the motors of aircraft); low resistance to peel stresses, difficult to dismantle bonded joints. Furthermore, bonded joints and the composite itself are difficult to inspect using NDT techniques because of the heterogeneous nature of the material, which causes serious problem for predicting optical and acoustic transmittance through the material because the fibers have widely varying dielectric properties from the resin matrix [16].

1.3 *Common flaws in aerospace composites*

A large percentage of flaws in composite materials occur at the bonded joints. These flaws can occur during manufacturing or during operation and can be identified as (See fig. 12) [20]:

- Porosity; which results from trapped gases and volatiles associated with the curing process.

- Voids; which may be formed by the coalescence of porosity, entrapment of air during application of the adhesive or by insufficient adhesive being applied
- Incorrect cure; this is caused by the presence of contaminants, bad formulation, or poor mixing of the adhesive.
- Cracks within the adhesive; these are generally associated with curing and thermal shrinkage during manufacture or handling and impact in use.
- A weak or non-existent bond; generally results from a contaminated substrate surface or if the adhesive is used too long after mixing.

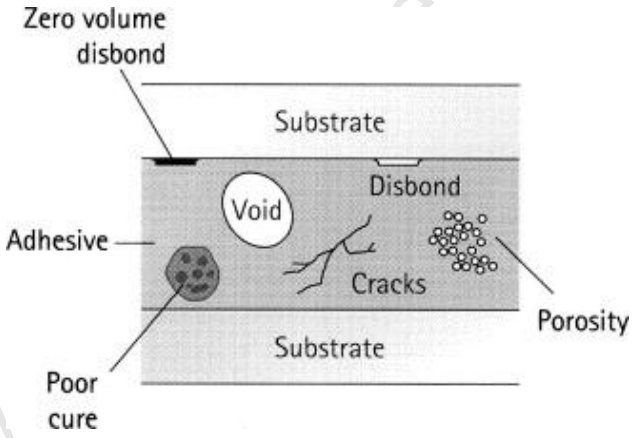

Figure 12: Potential defects in adhesive bond [17]

Composite laminate components are also prone to debonding/delamination when subjected to high interlaminar stress or when under impact. These repeated cyclic stresses and impact can cause layers to separate with significant loss of mechanical toughness. While delamination failure in itself is not usually catastrophic, its weakening influence on a component may lead to subsequent failure modes. Hence debonding or delamination may significantly reduce the strength of an aircraft or its fatigue life [21].

CHAPTER 2: NON-DESTRUCTIVE INSPECTION TECHNIQUES OF AEROSPACE COMPOSITES

Non-Destructive Inspection Techniques allow the inspection of a component without changing its characteristic form. NDT is now a relatively mature field, even though accurate characterization of hidden flaws may still pose some challenges. The requirements for NDT are continuing to be driven by the need for lower cost methods and instruments with greater reliability, sensitivity, user friendliness and high operational speed. In addition to these needs, the technology is sought for applicability to increasingly complex materials and structures.

There are many techniques as evidence in the literature used for NDT inspection, with the view that no single method can provide all the necessary information about the integrity of the material. With so many techniques commercially available, good knowledge of the NDT practice is required to decide which technique would be suitable for a specific application.

The basic information that is required in a defective material is the nature of the defect, the size and its location. Some of the NDT techniques in practice such as: Tapping, Ultrasonic, Eddy Current, etc. permit the determination of the location of the defects and possibly their size. Today with the advancements in the imaging technology, there exist more sophisticated NDT techniques that determine the location and size of the defect and also enable the operator a view of the defect in the material through the available imaging system. The most promising imaging NDT techniques that meet the required specifications and are commercially available as fully engineered systems are: laser ultrasonic, transient thermography and optical shearography and ESPI [4]. But in this project only optical shearography and ESPI will be discussed. To better understand these two techniques, the principle of holography and interference of fringes is of outmost importance.

2.1 Holography and Speckle Pattern Interferometry

Holographic interferometry is the interferometric comparison of two or more light waves, at least one of which is holographically reconstructed [25].

The theory of holography was first developed in 1947 by the British/Hungarian scientist Dennis Gabor while working to improve the resolution of an electron microscope. Using a mercury arc lamp, the non-coherent light source resulted in distortions in his images. The resulted images, he called holograms. The term hologram is taken from the Greek word ñholosòmeaning whole and ñgrammaò, meaning message or record [26].

Lacking a proper coherent light source, the interest for holography faded until the invention of the laser by Dr. T.H. Maiman in 1960. The monochromatic (one wavelength) and coherent (light in phase) output from the laser made it possible to produce distortion free holograms of high quality.

This technique enables the measurement of static and dynamic displacements of an optically rough surface through the use of interferometry which is possible because a light wave scattered by an object can be holographically recorded and reconstructed with such precision that it can be compared interferometrically with light scattered by the same object at another time [25].

With advancements in technology, the principle of holography has been employed to develop a dry type of interferometry known as electronic speckle pattern interferometry (ESPI). Further development of the basic technique has led to shearography, a more convenient set-up which measures displacement gradient directly.

2.1.1 Speckle Pattern

Speckle pattern is observed when an object is illuminated with coherent laser light. This is created by interference of wavelets of coherent light of different path length due to surface roughness. Each point on the illuminated object scatters some light to the observer. Because of the coherent nature of the laser light, the laser light scattered by a point interferes with the light scattered by other object points producing a speckle pattern. The random pattern of light interference is termed ñspeckleò The randomness is caused by the surface roughness because the phase of light scattered will vary from point to point in proportion to the local surface height [25].

The size of speckle viewed through a lens (Vest C, 1979), can be estimated by:

$$b_s \cong 1.22\lambda\left(\frac{f}{D}\right) \qquad Equation\ 3$$

Where b_s is the speckle width, f is the focal length of the lens in the imaging system, D is the diameter of the lens pupil and λ is the wavelength of the laser light. The speckle width of typical imaging systems vary from about $f/1.4$ to $f/32$. If the speckle pattern is formed by imaging scattered by He-Ne laser light ($\lambda = 632.8\ nm$), the corresponding speckle size varies from 1 to 24 µm [25].

2.1.2 Intensity Distribution of a Speckle Pattern

The intensity distribution I_b of the speckle pattern before deformation of the test object is given by the following equation: [27]

$$I_b = A_1^2 + A_2^2 + 2\sqrt{(A_1^2 A_2^2)}Cos(\theta_1 - \theta_2) \qquad \textit{Equation 4}$$

Where A_1 and A_2 are the complex amplitudes of the object and reference beam wavefront and $(\theta_1 - \theta_2)$ is the phase difference between the two wavefronts.

After the stress is applied to the test object, the intensity distribution I_a is represented by:

$$I_a = A_1^2 + A_2^2 + 2\sqrt{(A_1^2 A_2^2)}Cos[(\theta_1 - \theta_2) + \Delta\phi] \qquad \textit{Equation 5}$$

Where $$\Delta\phi = \frac{4\pi}{\lambda} = 2\pi m \qquad \textit{Equation 6}$$

$\Delta\phi$ Indicates the change in wavefront phase as result of the displacement of the object

The resultant intensity distribution I_r by the subtraction of the wavefronts is:

$$I_r = I_b - I_a = 4\sqrt{(A_1^2 A_2^2)}Sin[(\theta_1 - \theta_2) + 0.5\Delta\phi]Sin0.5\Delta\phi \qquad \textit{Equation 7}$$

While the addition of the wavefronts results in:

$$I_r = I_b + I_a = 2(A_1 + A_2) + 4\sqrt{(A_1^2 A_2^2)}Cos[(\theta_1 - \theta_2) + 0.5\Delta\phi]Cos0.5\Delta\phi \qquad \textit{Equation 8}$$

The two equations above (for determining the resultant intensity distribution) can be used successfully, but the subtraction of the wavefront intensities is preferred because under this condition, black fringes are created (the imagesô intensity cancels out as a result of phase change from the surface displacement).

2.2 *Electronic Speckle Pattern Interferometry (ESPI)*

Electronic Speckle Pattern Interferometry (ESPI) is an optical laser based, non-contact, whole field non-destructive testing technique that responds to changes of surface topography (surface displacement) caused by the action of an external force, pressure changes or by thermal expansion. Hidden defects are revealed by the inhomogeneity of such deformation fields. Unfortunately, field distortion may also be caused by other factors including inhomogeneous excitation [28].

In using ESPI, an image of the objectôs surface is obtained at any given stress level and stored in the computer. After a minor perturbation of the object by an applied stress, which may be heat applied by blowing hot air to the surface, a minute pressure exerted, vacuum applied or through vibration, a second image is obtained and stored in the computer. Appropriate software allows the addition or subtraction of the pixels of the two images, giving rise to interference fringes which represent the difference in surface dimensions between the two images of the object under test [29].

The surface displacement can be measured either in the in-plane or out-of-plane direction depending by the choice of the sensitive arrangement on the set-up of the optical components of the ESPI system. The out-of-plane displacement sensitivity arrangement is the more versatile of the two as it makes better usage of the light emitted by the laser.

The set-up arrangement for ESPI (See fig.13) comprises of a laser source, which generates a single mode monochromatic laser that is used to produce the speckle interference. The interferometer consists of two laser beams, generated by passing a single laser beam through a beam splitter. The first beam is the object beam and is passed through a beam expander and is used to illuminate the object. The second beam is the reference beam; this is directed via a set of mirrors onto the image recording medium, typically a CCD camera. With the camera focused on the testing object, the beam path of the object and reference beam will overlap. The interference of these two beams will produce a speckle pattern which is recorded

by the CCD camera. With the aid of a frame grabber, the images are captured and stored in the PC.

By comparing the speckle images of the object captured before and after stressing, areas of correlation and decorrelation can be determined, which when mapped, produce a zebra-striped fringe pattern. The following equation (eq. 9) can be used to represent the surface displacement mathematically. [30]

$$d = \frac{n\lambda}{\cos\alpha + \cos\beta} \qquad Equation\ 9$$

Where d is the out of plane displacement of the object normal to the surface, n is the number of fringes observed, λ is the wavelength of the laser light used, and α and β are the angles between the object's surface normal, and the observer and the direction of the object illumination beam.

For small angles of camera viewing and object illumination beam, the above equation can be simplified to:

$$d = \frac{n\lambda}{2} \qquad Equation\ 10$$

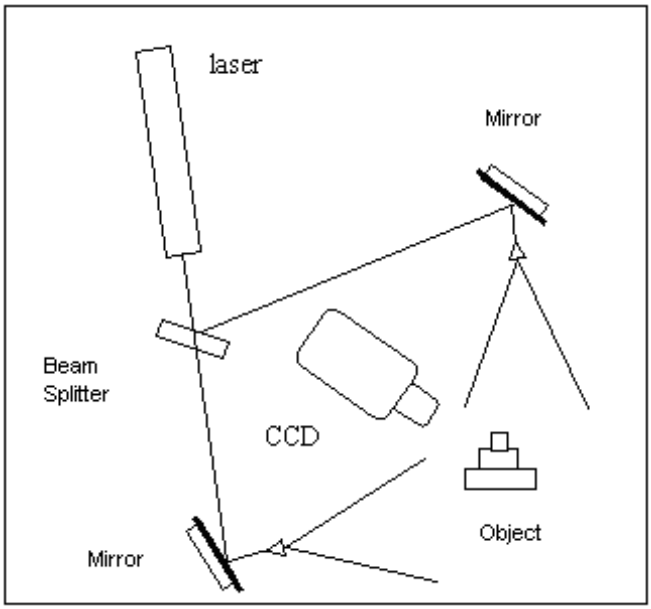

a) In-plane ESPI

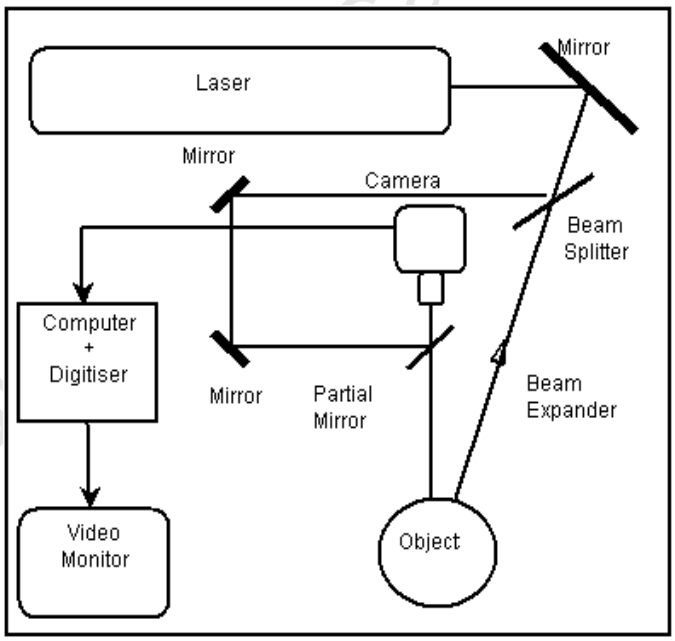

b) Out-of-plane ESPI

Figure 13: ESPI set-up arrangements

2.3 *Shearography*

Digital Shearography is also a laser based, full field, non-contact optical interference technique used primarily for strain measurements and NDT. The result of this testing technique is a set of fringe patterns which represent the gradient of an object's surface displacement in response to an applied stress. The presence of a defect locally influences the object's surface deformation when stressed and this can be detected in the contours of the produced fringe pattern.

The optical configuration used for digital Shearography (See fig. 14) utilizes similar optical components as in the ESPI set-up. The difference is that for digital Shearography, the beam emitted by the laser is not split into an object and reference beam. Instead, the emitted laser beam is expanded and used solely to illuminate the object. The monochromatic laser light, which reflects off the illuminated object surface, is viewed through a set of shearing optics. The function of the shearing optics is to laterally shear the image of the object into two overlapping images.

The images are obtained before and after a mild stressing of the object. The stressing changes the dimensions of the object which in turn has an effect on the intensity of the speckled image. The addition or subtraction of the images gives rise to interference fringes which will represent the gradient of surface displacement. Mathematically, the fringes can be represented by the following equation: [31]

$$\Delta\phi = \frac{4\pi}{\lambda}\left(\frac{\partial d}{\partial x}\right)S \qquad \textit{Equation 12}$$

Where: $\Delta\phi$ is the correlation phase, $\frac{\partial d}{\partial x}$ is the gradient of surface normal displacement, S is the magnitude of shear and λ is the wavelength of the laser light. The correlation phase $\Delta\phi$

is constant and represents lines of constant displacement rate. The spacing between adjacent fringes is a function of the displacement gradient given by:

$$\frac{\partial d}{\partial x} = \frac{n\lambda}{2S}$$ Equation 13

Where: n = no of fringes

From the above equation it can be concluded that for a given object surface area, an increase in displacement gradient will produce a corresponding increase in number of fringes.

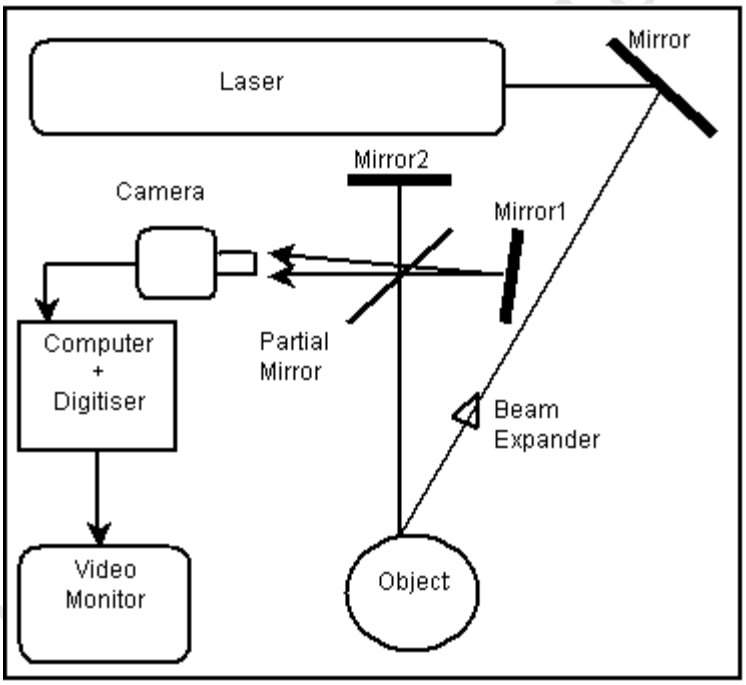

Figure 14: Typical Shearography set-up for surface normal displacement gradient

2.4 *Phase Stepping*

Phase stepping is a technique used in interferometry to recover the optical phase from the intensity. This is achieved by measuring the intensity phase at a minimum of three phase steps and the individual intensities are combined to yield the wrapped phase [32].

Phase steps are produced by the mechanical micro-displacement of a calibrated piezo-electrically driven mirror. The micro-displacements are produced by applying a voltage across the piezo-electric crystals which results in their expansion. Each micro-displacement of the piezo-electric mirror actuates phase-steps of ´ /2 increments for a 4 image configuration, which is equivalent to changing the path length of the laser beam by a quarter of a wavelength between each of four images captured before and again after the test specimen has been stressed. Custom software is developed to control the actuator power supply, as well as the image acquisition, manipulation and display routines. [33]

To determine the intensities and the phase distribution of the speckle interference pattern, the following equations are used:

$$I_i(x,y) = I_B(x,y) + I_{MP}(x,y)\cos(\theta(x,y) + i.\pi/2) \qquad \textit{Equation 14}$$

$$\emptyset(x,y) = arctan\left(\frac{I_3(x,y) - I_1(x,y)}{I_4(x,y) - I_2(x,y)}\right) \qquad \textit{Equation 15}$$

$$\beta(x,y) = \emptyset_a(x,y) - \emptyset_b(x,y)$$

Equation **16**

Where: i = 1,2,3,4

$\emptyset_a(x,y)$= phase distribution after stressing

$\emptyset_b(x,y)$= phase distribution before stressing

$\beta(x,y)$= change in phase of the laser light due to the object surface displacement

The phase difference lies within 0 to 2´ and repeat itself after 2´ intervals. After the phase difference is calculated using the customized software, a phase map is produced consisting of fringes changing from black to white and back to black again. This occurrence result in a ñsaw toothò pattern (fig. 15b) which continues throughout the image and is due to the phase difference increasing towards 2´ and then jumping to zero when the limit of 2´ is reached. The 2π ambiguity is then removed using phase unwrapping techniques to obtain, in the case of shearography, the displacement gradient in the shear direction across the surface of the object.

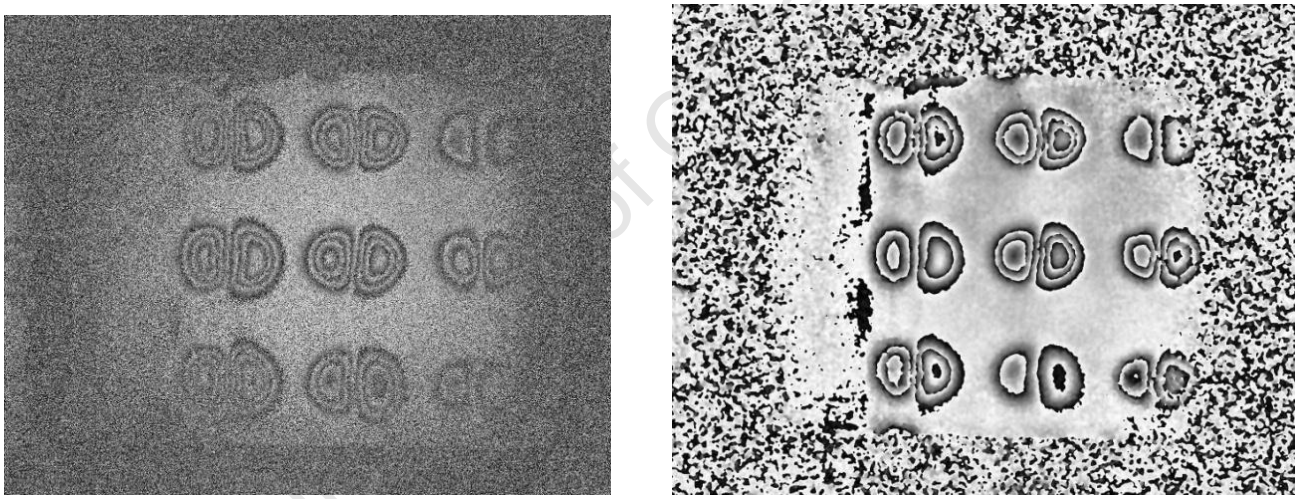

(a) (b)

Figure 15: (a) Intensity fringe pattern, (b) Filtered phase fringe pattern

CHAPTER 3: EXCITATION OF AEROSPCE COMPOSITES FOR NDT

The excitation of composite materials is dependent on the chosen NDT technique. Researchers in the NDT department at the University of Cape Town (UCT) are focused in Shearography and ESPI as the NDT techniques of choice. To test the integrity of a material using either of these methods, the material needs to be excited (stressed). When a component with a defect is stressed, there will be higher energy concentration at the location of the defect and the interference between the stressed and unstressed position will permit the exposure of the defect.

Researchers at the NDT department at UCT have also considered a number of ways that a material can be stressed for NDT with Shearography or ESPI which can be: applied heat with a lamp or hair dryer, vacuum, sound, etc.

Heating has thus far proven to be the more convinient way of stressing the material under test with either Shearography or ESPI. But as new materials evolve and testing may need to be done in an environment sensitive to heat, alternative means of excitation need to be developed. The proposed method which has not seen many applications is vibration excitation.

3.1 *Vibration Excitation*

Vibration excitation is accomplished by introducing a forcing function into a structure, usually with some type of shaker or transducer. Shakers are usually used to induce the vibration

because parameters such as frequency, wave length and amplitude can be controlled and determined with fair accuracy.

The principle of vibration that is of interest as a possibly viable excitation technique for ESPI and Shearography is that the vibration field will cause the defect interfaces to rub. This action (friction) will generate heat, resulting in a localized increase of temperature which in turn will affect the surface displacement. It is expected that resonance frequency and sufficiently high enough amplitudes should be effective in exposing small cracks and delaminations.

3.1.1 Vibration Wave Propagation in Solid Structures

All material substances are comprised of atoms, which may be forced into vibration motion about their equilibrium positions. The vibration wave induced by a shaker to a certain extent is similar to that induced through ultrasound or acoustics. The oscillating variation propagates in the form of a wave. A wave travels through a medium, transporting energy from one location (its source) to another location. Each individual particle of the medium is temporarily displaced and then returns to its original equilibrium position. The energy transported by a wave is proportional to the square of the amplitude of the wave according the following equation. [22]

$$E_t = \frac{1}{2}kA^2 \qquad Equation\ 17$$

Where *k* is the stiffness of the material and *A* the amplitude of the wave; likewise, the rate of energy transfer or the average power is proportional to the frequency of vibration; expressed mathematically as:

$$P_{avg} = \frac{1}{2}kv\omega^2A^2 \qquad Equation\ 18$$

The dissipated energy value in a complete loading cycle is calculated in the following way [23]:

$$W_d = \frac{Q}{t\omega} \qquad Equation\ 19$$

$$Q = m\Delta T \qquad Equation\ 20$$

Where W_d is the dissipated energy, υ is the frequency of the steady state vibration, v is the wave speed, Q is the heat energy gained measured by a calorimeter, t is the time taken, ΔT is the temperature difference and m is the mass of the substance.

Since the dissipated work is transformed into heat energy, for every cycle the temperature will rise accordingly:

$$\Delta T = \frac{W_d}{\rho C_p}\Delta t \qquad Equation\ 21$$

Where Δt is time period per cycle, and C_p is heat capacity and ρ is the density of the material

The speed of the wave through a solid material (e.g. a rod), for a longitudinal wave can be defined with the following equation:

$$v = \sqrt{\frac{E}{\rho}} \qquad Equation\ 22$$

Where E is the elastic modulus of the material

The wave speed can also be expressed in terms of the wave length and the frequency as in the following equation:

$$v = \lambda f \qquad Equation\ 23$$

Where λ is the wave length and f the frequency of the wave

In several cases a small damage in structures does not influence the static response or the small amplitude vibration response of the structure. However, its influence can be observed

when the structure is subjected to large dynamic loads, leading to large amplitude vibrations. In this case even small changes in the structure (like cracks and other local damage scenarios) can have a considerable effect on the structural response in the time domain, which in turn can give an indication of the presence of the damage.

Cases when the frequency of excitation is close to one of the first natural frequencies of the system the vibrating systems are usually quite sensitive to even small changes introduced in their geometry or the physical properties including damage. These regimes of large amplitude vibrations are therefore expected to enhance the sensitivity of nonlinear vibrating structures to damage, even though the changes in the natural frequencies might be negligible [24].

3.1.2 Practical Applications of Vibration Excitation for NDT

The vibration-based structural damage detection is one of the techniques in use to detect defects throughout the whole body of large complicated structures. This technique is based on the principle which views any structure as a dynamic system with stiffness, mass and damping. Once a defect emerges in the structure, the structural parameters will change, and the frequency-response function and modal parameters of the structural system will also change. Thus, the change of the structural modal parameters can be taken as the signal of damage occurrence. [37]

In the past, the vibration-based structural damage detection method was mainly based on the natural vibration characteristics of the structure (natural frequency, or mode shape). When the measured data of the natural frequency or mode shape are different from those of the intact system, it indicates the damage emergence in the structural system. In the industries today, vibration excitation is used for several NDT techniques, among them are the following: [37]

- **Method based on the structural vibration mode:**

Structural damage existence can be detected through the natural frequency change and information about the vibration modes may help locate the structural damage.

The advantage of using the change of structural natural frequency to detect damage is because it is a convenient measurement of high accuracy. However, the measurement of natural frequency cannot provide enough information for structural damage detection. Furthermore, the natural frequency is often not sensitive enough to initial damage in structures. Usually, this method can only ascertain the existence of considerable damage, but may not be able to give the damage location because structural damage in different location may cause the same frequency change.

- **Method based on the change of structural flexibility or stiffness:**

  When a defect appears in a structure, the stiffness can offer more information than the mass. Using the changes of stiffness to detect damage is because the stiffness changes remarkably when damage occurs in a structure. However if the damage is very small, this method more likely would not work well.

- **Wavelet analysis method:**

  This technique is executed by comparing the discrete wavelet transforms of two sets of vibration signals from the undamaged and damaged structures in the space domain, not only the presence of defects can be detected, but also their number and location as well.

- **Artificial Neural Network method:**

  To evaluate a structure, using the neural network method, the known feature information (NN input) and the corresponding status (NN output) of structural damage are taken as guide samples to train the constructed NN. This damage information or train sample can be obtained by experiments or numerical simulations. When the NN

has been well trained, one can input the experimentally measured real structural damage feature index in to the trained NN, and the output of the trained NN will be able to give the location and severity of the structural damage.

- **Adaptation of vibration excitation to optical Shearography and ESPI**

  The success of vibration excitation in the above mentioned NDT techniques has inspired its adaptation to optical Shearography and ESPI, but in this occasion the main aim of the vibration is to generate heat in the material and expose the defects.

CHAPTER 4: METHOD OF INVESTIGATION

To fully understand how well vibration excitation works, in conjunction with ESPI and/or Shearography for defect determination in aerospace composites, one will have to test all the different composites used in the aerospace industry and all the possible defect scenarios. Unfortunately this is not feasible as the number of composites used in the industry is very broad and everyday there is a new breed of composite material developed for the industry to enhance specific features. For this reason, this investigation has been limited only to fiber reinforced composites (FRC) from which five main composites have been chosen for their popularity in the industry (CFRP, GFRP, Carbon laminates, and Perspex), to be used to manufacture the test specimens.

The main equipment that will be used for the investigation are the traditional ESPI/Shearography systems available in the NDT laboratory at UCT (see fig.17 and 20). The additional components introduced for this particular investigation are: function generator and a shaker

4.1 *The Vibration Generator (Shaker)*

The vibration generator (see fig. 16) to be used in this project is basically a loudspeaker. This shaker is an electro-magnetic vibrator, designed by ***Frederiksen Ltd***, a robust and versatile apparatus well suited for all sorts of wave experiments.

A function generator is to be attached to the shaker through the provided banana plugs connection for the purpose of generating waves. The Vibration Generator will vibrate at any frequency ranging from 0.1 Hz ï 5 kHz and with amplitudes up to 7 mm at the low end of the

frequency range. The waveform need not be a sine wave; other waveforms such as square, triangular or sawtooth can be used.

A safety feature in this vibration generator is the ñock/unlockò mechanism, when set in the lock position the center-tap is locked, and accessories can be mounted without any damage to the moving parts.

This vibration generator was usually operated via a function generator that could only put out 1.5 W of power. To run the shaker at its maximum output power, a new function generator was acquired which can put out up to 100 W of power, with output frequency range up to 15 kHz. This was desirable because energy is transfered to the specimen at a faster rate which in turn will reduce the time required to expose the defects.

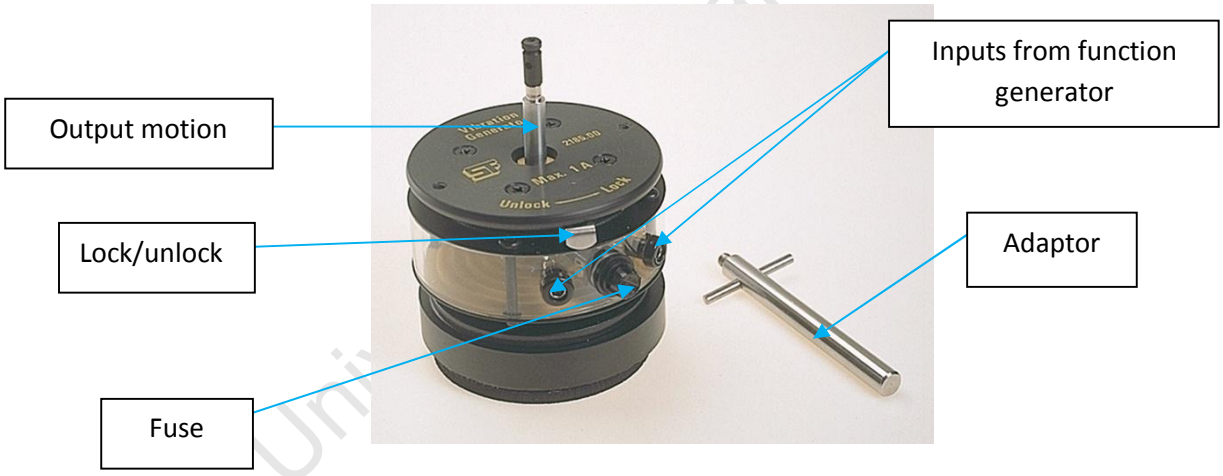

Figure 16: Vibration generator

Table 1: Technical specifications of the vibrator generator

Frequency range	0.1 Hz to 5 kHz
Amplitude	7 mm at 1 Hz, decreasing with increasing frequency
Input impendance	8 ohm
Max. Inputs	6V/1A
Dimensions ű	100 x 120 mm
Weight	1.2 kg

4.2 *Testing Set-up*

4.2.1 Shearography set-up

The Shearography set-up as illustrated schematically in fig. 14 was assembled on the optical table available in the UCT NDT laboratory as depicted in fig. 17.

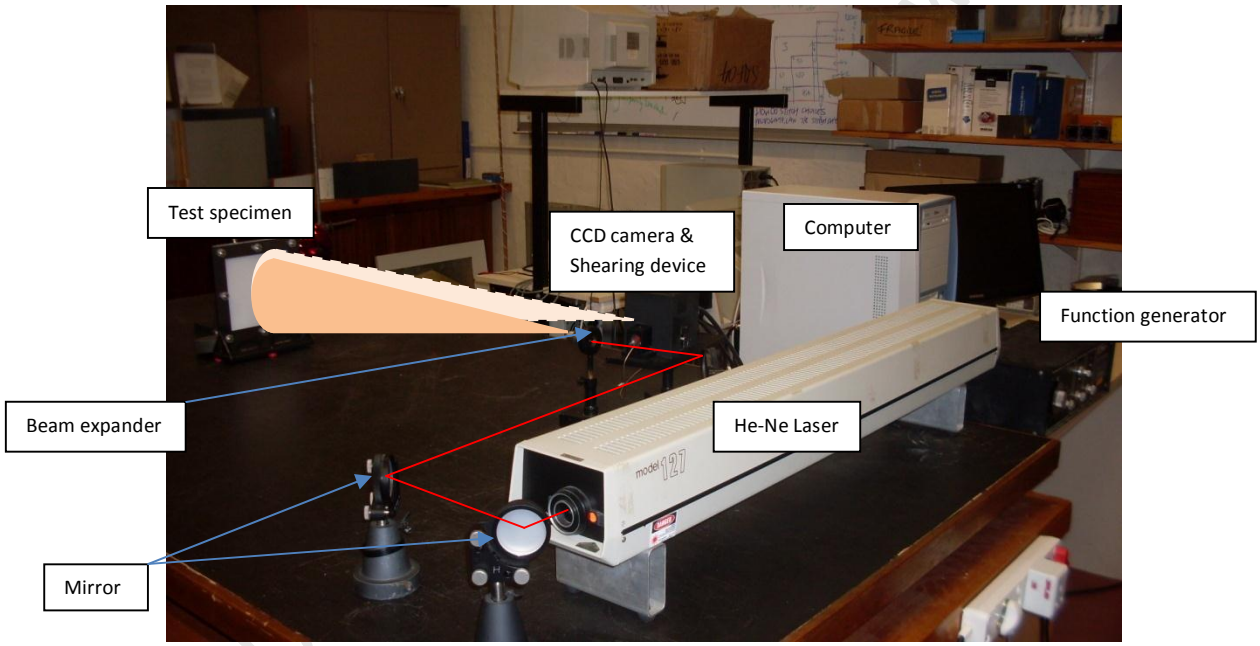

Figure 17: Laboratory set-up for Shearography tests

The vibration generator was placed with its output protruding shaft touching the surface of the test specimen (see fig. 18). Once the specimen was excited, the vibration generator was turned off and the Shearography equipment was ready to detect any defects that may have been exposed by the energy induced through the vibration excitation.

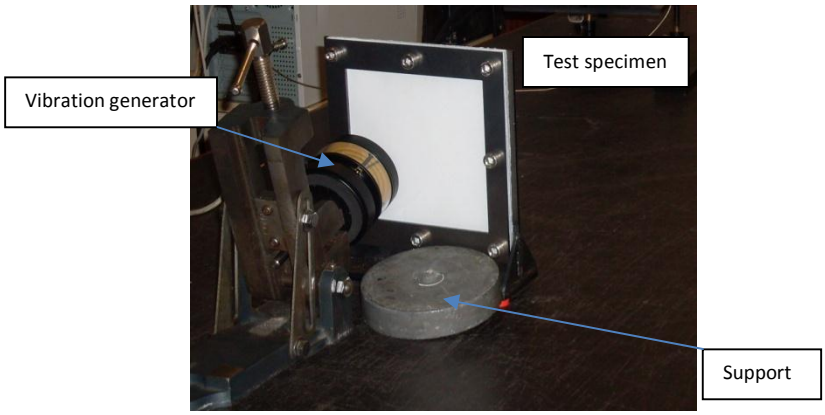

Figure 18: Vibration excitation of the test material

During Shearography and ESPI testing, excitation through mild heating from past experience has proven to be more efficient in exposing flaws and defects in materials. To understand how effective vibration excitation is in exposing defects, comparison is to be established with the heating excitation. At UCTôs NDT laboratory, two methods of heating technique are currently used: heating by radiation from a glowing lamp and heating through a hair-dryer (see fig. 19). For comparison purposes with the vibration excitation technique, either of these heating methods will be used.

a) Lamp heating

b) hair-dryer heating

Figure 19: heating excitation techniques

4.2.2 ESPI set-up

The schematic for ESPI set-up was illustrated in fig. 13. The out-of-plane configuration (fig. 13b) will be adopted for testing. This configuration was assembled on the laboratory optical table as illustrated in fig. 20 below.

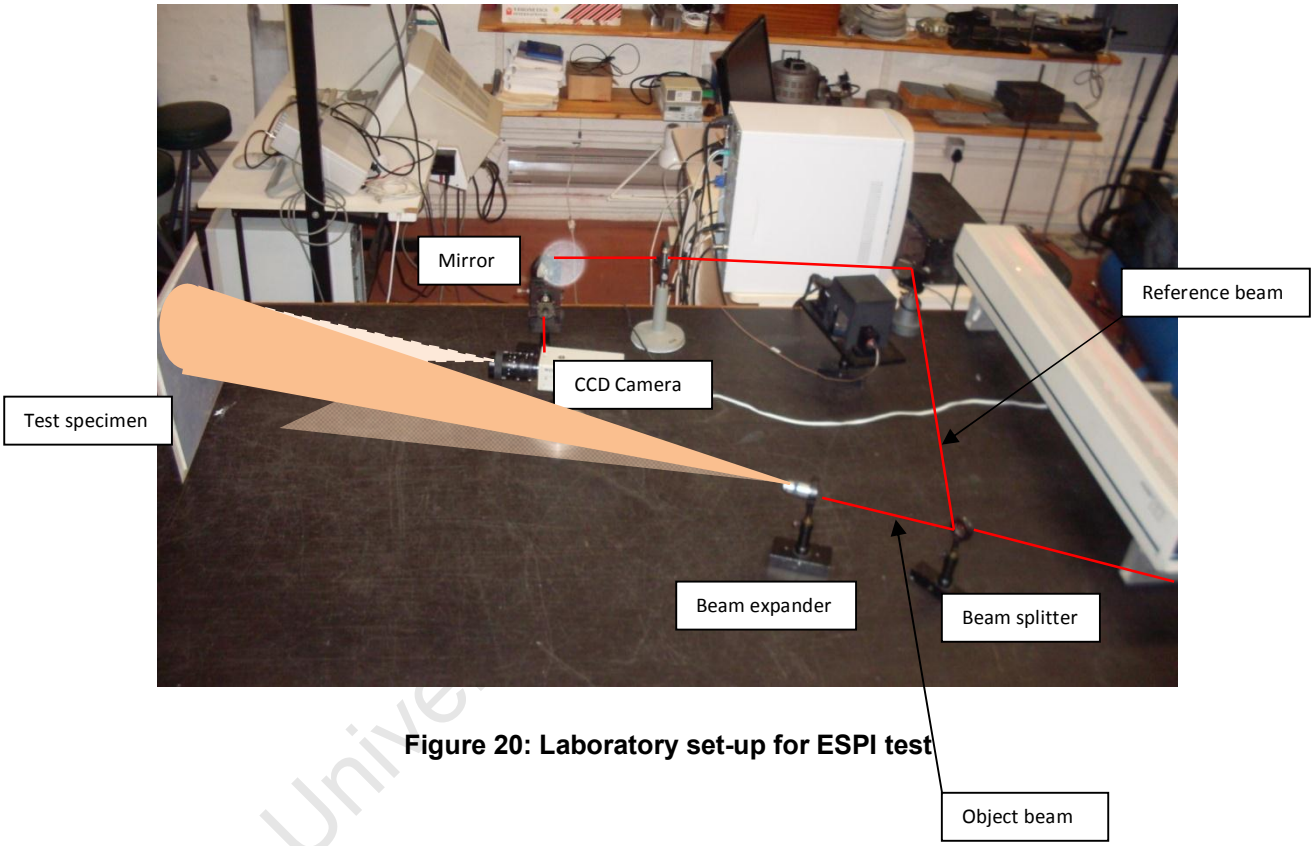

Figure 20: Laboratory set-up for ESPI test

Careful measurements are required in setting-up the ESPI configuration, making sure that the reference beam path from the beam splitter to the CCD camera is equal in length to the path taken by the object illumination beam to the CCD camera. This will permit both laser beams to have the same coherent length at the intersection in the CCD camera which will allow for better fringe image resolution.

CHAPTER 5: TESTING

The composite specimens build as prototypes of typical aerospace composites, were manufactured with either internal or external predefined defects. These specimens were non-destructively tested using the ESPI and/or Shearography techniques after a mild vibratory excitation. The objective was to find the level of excitation which would invoke a response from the defects, differentiating them from the immaculate parts of the specimen.

5.1 Real time ESPI/Shearography with vibration

Before applying vibration excitation to the selected specimens for NDT with ESPI and/or Shearography, tests were conducted to understand how the exposure of the defects with vibration excitation was affected by the following variables:

- Frequency and amplitude of vibration
- Duration of vibration excitation

5.1.1 TEST 1: Determination of the frequency and vibration time duration

Because each composite material presents unique properties, the frequency, amplitude and vibration time duration required to expose the defects would be determined individually for each specimen. The following experiment illustrates the procedure that was followed to accomplish this task.

The Nomex honeycomb core helicopter rotor blade in fig. 21 was selected for this experiment. This specimen contains 9 circular holes of equal diameter but varying depth that were studied in further detail later in this project but for this experiment, only the centre hole (no. 5) would be of interest.

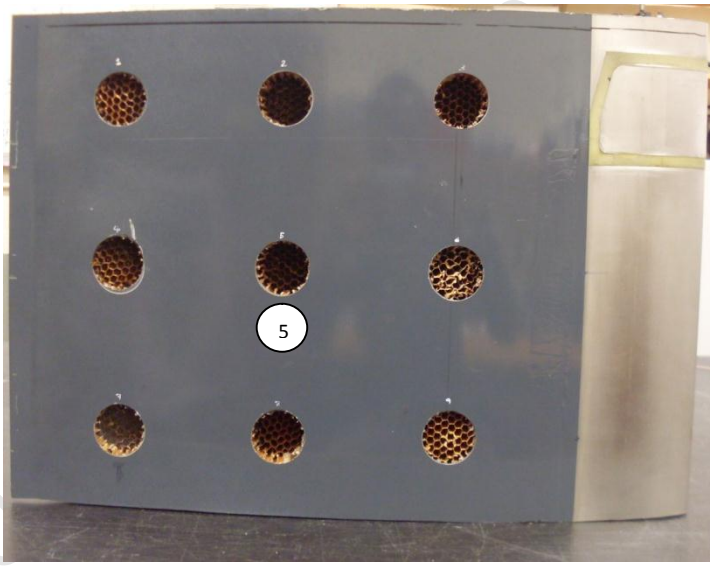

Figure 21: Nomex honeycomb core helicopter rotor blade panel

Hole no. 5 was tested independently and the aim was to illustrate the procedure that would be followed to determine the frequency, amplitude and vibration time duration required to expose defects in the selected specimens. The diameter of the hole is 45 mm, the depth is 40 mm, and the distance from the viewing surface is 13 mm.

The Experiment

The panel was placed on the optical table and a Shearography test was conducted. Prior to this, the panel was excited with vibration, with the vibrator placed at the back of the panel right on the hole in question.

With the vibrator in place, the testing started with a checklist sheet presented in Table 2, as a guide to select a frequency and vibration time duration. A stopwatch was used to monitor the time for the excitation. Throughout the excitation, the amplitude was kept as high as possible to induce the highest amount of energy available at the selected frequency in order to expose the defects in the shortest time.

After the excitation the panel was viewed through the Shearography unit and marked accordingly in the checklist to indicate whether the defect was visible or not. Another aspect of this test was to determine the minimum excitation time required to expose the flaw with the lineup frequencies. For this reason three excitation times (2, 5 and 10 min) were selected to be matched against the increasing range of frequencies as can be seen in the checklist table. In this table, the following notations were used to quantify the visibility of the defect after each excitation.

Defect not visible → ✗

Defects start to reveal → ✓

Defects visible but not fully developed → ✓✓

Good and clear visibility of defects → ✓✓✓

The above notation was awarded after each test, for example: in Table 2, the first test was conducted at 10 Hz and 2 minutes vibration duration. At the end of this excitation the defect was not visible, and therefore the corresponding box for the combination was marked ✕. Because the aim was to minimize the vibration time, only the frequency was increased to induce more energy and expose the defect. The next test was conducted at 25 Hz and 2 minutes vibration duration, at this point the defect started to reveal and the corresponding box was marked ✓. The frequency was increased again and the next test was conducted at 50 Hz and 2 minutes vibration duration; still the visibility of the defect was not good enough but better than the previous excitation therefore the corresponding box was marked✓✓, the frequency was increased again until the defect was clearly visible at 100 Hz and the corresponding box was marked ✓✓✓.

For the frequencies that revealed the defect but not clear enough, the excitation time was increased (i.e. 25 Hz and 5 minutes) until the defect was visible at that frequency. But the bottom line was that the frequency that revealed the defect in the shortest time was desirable.

In between the excitations, 2 minutes were allowed for the material to dissipate the energy absorbed from the previously excitation.

Table 2: Hole no. 5 (depth = 40 mm and distance from viewing surface = 13 mm)

	Time (min)						
Frequency (Hz)	2	5	10	15	20	30	30+
10	✗	✓	✓✓				
25	✓	✓✓	✓✓✓				
50	✓✓	✓✓✓					
75	✓✓						
100	✓✓✓						
150							
250							
500							

The process described above will be followed for every vibration excitation test in this project to determine the frequency and vibration excitation duration; the amplitude will be kept as high as it can be with the corresponding frequency. Tests were not conducted beyond 100 Hz because as the frequency was increasing the amplitude was decreasing, causing the vibrator to lose contact with the panel after 100 Hz.

5.2 Shearography and ESPI testing of the selected specimens after vibration excitation

The basic types of fiber reinforcement materials (FRP) most commonly used in the aerospace composite industry are glass fiber, carbon/graphite and aramid fiber.

Core materials that form the basis of a sandwich composite structure range from balsa, formed plastics and highly engineered honeycomb structures.

In this project, the selected specimens for testing were sandwich composites with either Carbon Fiber Reinforced Plastic (CFRP) or Glass Fiber Reinforced Plastic (GFRP) as the skin material and Nomex Honeycomb or PVC foam as the core material. Perspex and Polycarbonate were also selected to form laminate composite specimens.

These specimens were carefully selected because of their wide range of applications in the aerospace composite industry and the induced defects where strategically placed so that the following could be investigated:

- The response of different composite materials to vibration excitation for NDT with ESPI and Shearography
- Response of different size defects to vibration excitation
- And the response of different defect depth location to vibration excitation

5.3 Fiber Reinforced Plastic (FRP) composite sandwich with Nomex Honeycomb core

In the aerospace industry, the most common honeycomb core is the PN2 aerospace grade aramid fiber honeycomb. It exhibits outstanding non-flammability properties. It is manufactured from DuPont Nomex® paper (or equivalent) and coated with a heat resistant phenolic resin. In addition, it is compatible with most adhesives used in sandwich composites.

Two main FRP materials are often used as the skin in the building of a sandwich composite with Nomex Honeycomb core, and these are: Carbon Fiber Reinforced Plastic (CFRP) and Glass Fiber Reinforced Plastic (GFRP) (see fig.22).

The applications of this type of sandwich composite in the aerospace industry include aircraft galleys, flooring, partitions, aircraft wing leading and trailing edges, missile wings, radomes, antennas, military shelters, fuel tanks, helicopter rotor blades and navy bulkhead joiner panels [35].

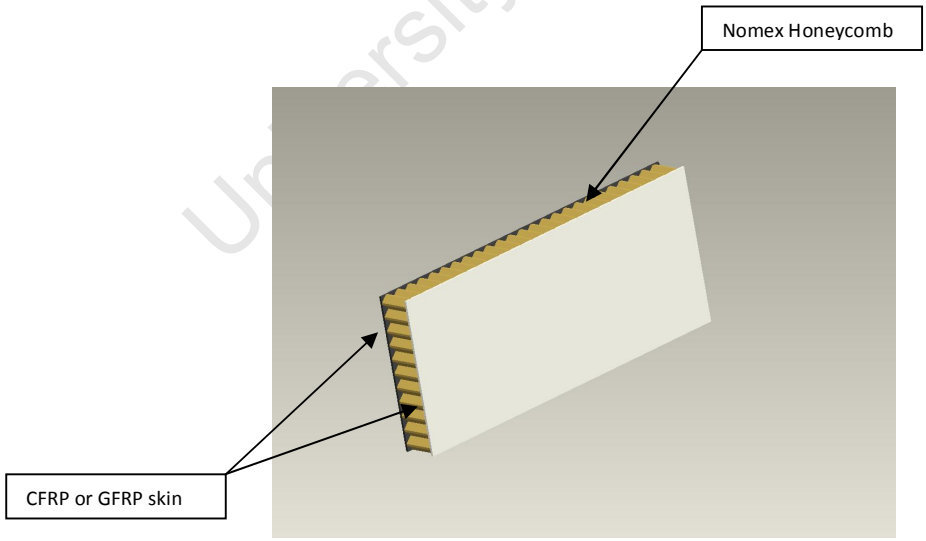

Figure 22: Nomex Honeycomb sandwich composite

5.3.1 TEST 2: Response of different size defects to vibration excitation

The specimen depicted in fig. 23 is a composite sandwich material of CFRP skin and Nomex Honeycomb core, cut-out from a helicopter rotor blade which was made available to the department. The defects induced in this specimen were four circular external voids of varying diameter (10, 15, 20 and 25 mm) and at equal depth (15 mm) from the viewing surface. The total thickness of the specimen is 20 mm (see Table. 3).

The aim when experimenting with this specimen was to observe how the size of the defect could influence the detection and the type of fringe pattern that this particular type of defect would exhibit.

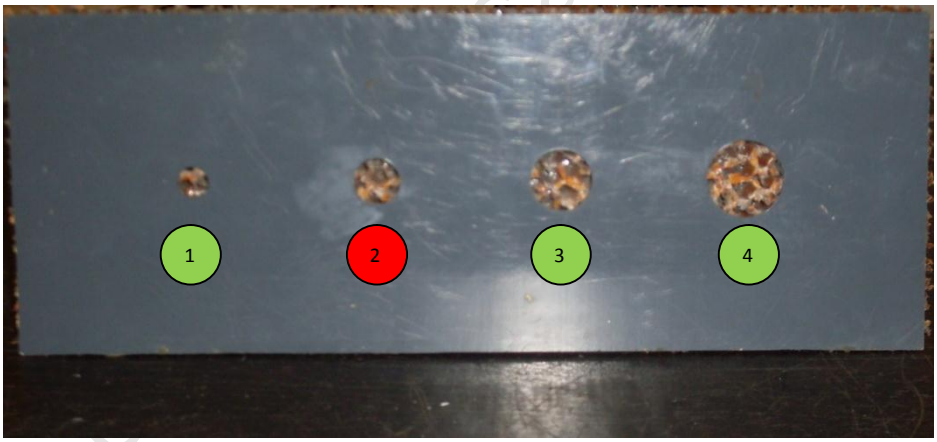

Figure 23: Specimen of CFRP skin and Nomex Honeycomb core with circular defects of varying diameter

Table 3: Dimension for specimen with circular defects of varying diameters

Hole no.	Thickness of specimen (mm)	Depth (mm)	Diameter (mm)
1	20	15	10
2			15
3			20
4			35

Three holes were selected from the specimen in fig. 23 to test for the efect of the size of the defect, numbered (1, 3 and 4) and marked with a green circle. The specimen was placed on the optical table and each hole was tested independently. Checklist tables were also used to evaluate each hole as it was undergoing the testing to determine the frequency, amplitude and vibration excitation time required to expose the defect. The results of the evaluation are recorded in Tables. 4, 5 and 6.

Table 4: hole no. 1 (diameter = 10 mm)

	Time (min)						
Frequency (Hz)	2	5	10	15	20	30	30+
10	✗	✗	✓✓	✓✓✓			
25	✗	✓✓	✓✓✓				
50	✓✓	✓✓✓					
75	✓✓✓						
100							
150							
250							
500							

Table 5: hole no. 3 (diameter = 20 mm)

	Time (min)						
Frequency (Hz)	2	5	10	15	20	30	30+
10	✓	✓✓	✓✓✓				
25	✓✓	✓✓✓					
50	✓✓						
75	✓✓✓						
100							
150							
250							
500							

Table 6: hole no. 4 (diameter = 35 mm)

	Time (min)						
Frequency (Hz)	2	5	10	15	20	30	30+
10	✓	✓✓	✓✓✓				
25	✓✓	✓✓✓					
50	✓✓✓						
75							
100							
150							
250							
500							

The circled boxes are the frequency and time combination that exposed the defects reasonably well. The graphical representation of these results is presented in fig. 24.

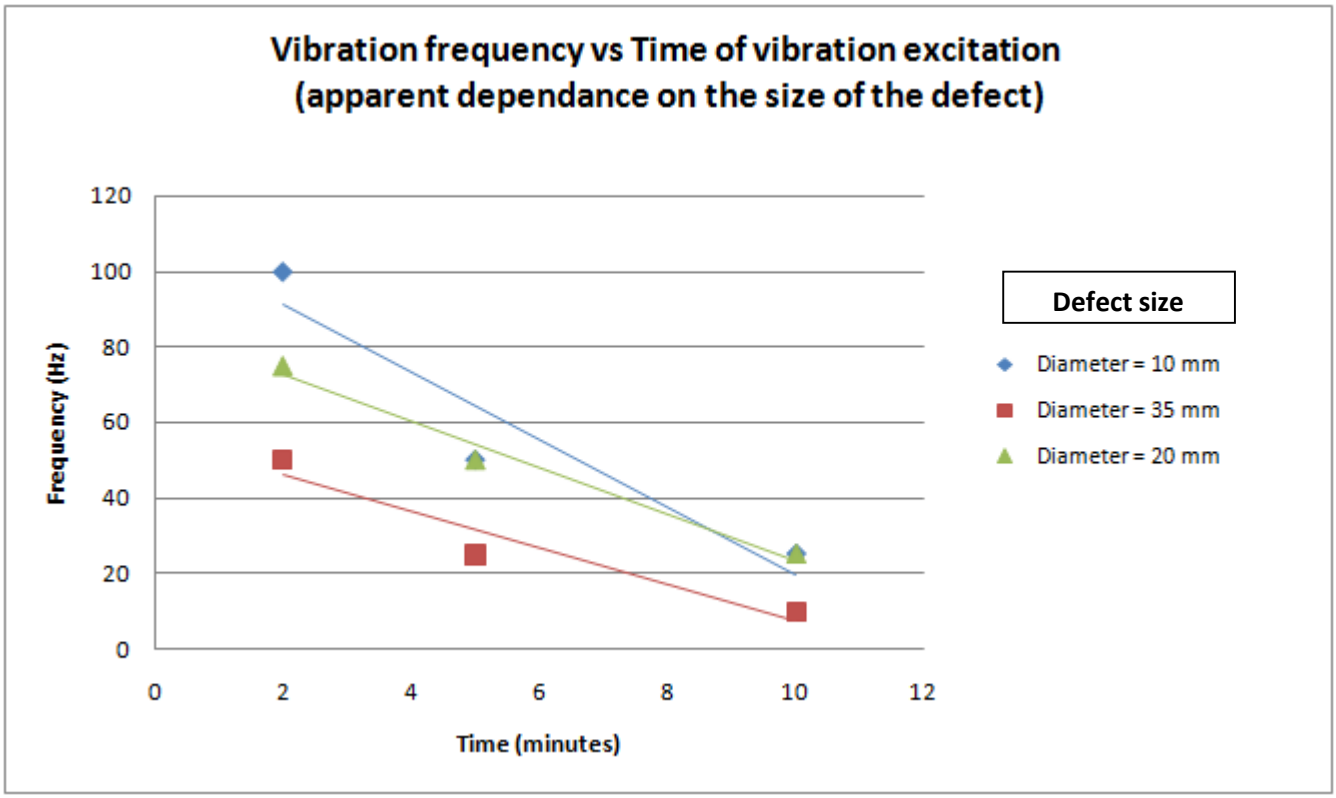

Figure 24: Vibration frequency vs Time of vibration excitation apparent dependence on the size of the defects

The relationship between the frequency and vibration excitation time shown in fig. 24 indicates that more energy is required to expose smaller defects with the same vibration excitation duration. For example, to expose the smaller defect with 2 minutes vibration excitation, it required higher frequency. The fringe images of the selected holes and the respective frequencies and vibration time duration are tabulated in Table. 7.

Table 7: fringe images of selected holes in fig. 24

	Hole no. 1 (diameter = 10 mm)			**Hole no. 3 (diameter = 20 mm)**			**Hole no. 4 (diameter = 35 mm)**		
	Frequency (Hz)								
Time (min)	25	50	100	25	50	75	10	25	50
2									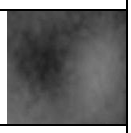
5		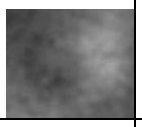			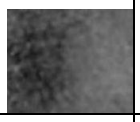			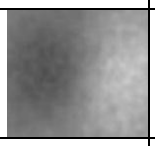	
10				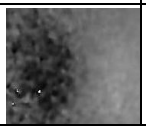					

With the knowledge of the frequencies and time of vibration excitation required to expose even the smaller defect, a test can now be performed on the specimen depicted in fig. 23 using vibration excitation with either ESPI or Shearography. The frequency of 100 Hz and the vibration duration of 5 minutes, yielded images that displayed all the defects (see fig. 25b and 26b).

a) ESPI tests

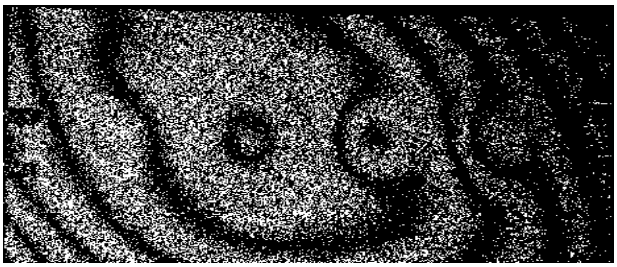

i) ESPI (3 sec heat excitation)

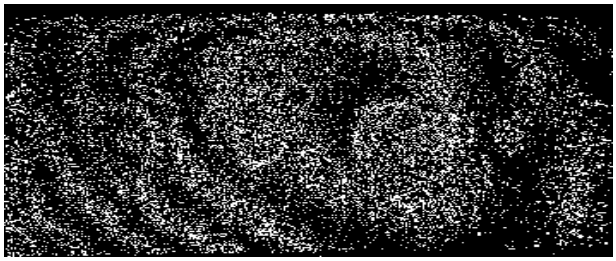

ii) ESPI (vibration excitation at 100 Hz & 5 minutes)

Figure 25: Fringe images resulted from ESPI tests of the specimen of CFRP skin and Nomex honeycomb core

b) Shearography tests

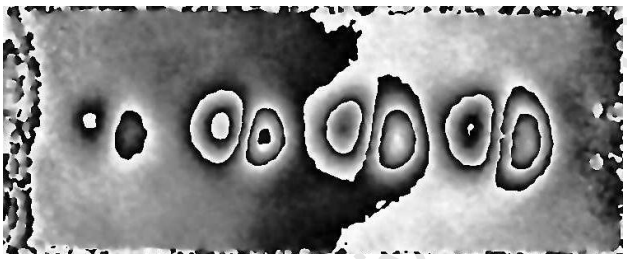

i) Shearography (3 sec heat excitation)

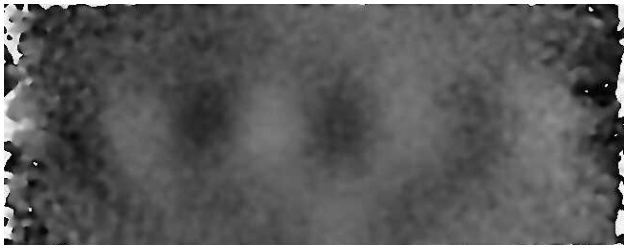

ii) Shearography (vibration at 100 Hz & 5 minutes)

Figure 26: Fringe images resulted from Shearography tests of the specimen of CFRP and Nomex honeycomb core

As mentioned before, in order to transmit high enough energy, high frequency coupled with high amplitude is required. High amplitude and frequency is not recommeded in that the impact can induce unwanted defects on the specimen (see fig. 27).

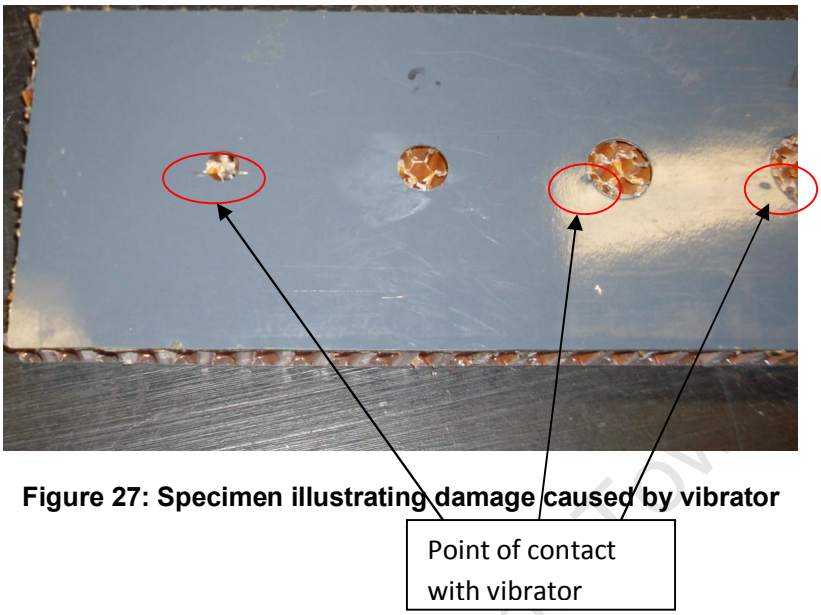

Figure 27: Specimen illustrating damage caused by vibrator

In fig. 27, red circles illustrate the specimen's surface as damaged by the vibrator from the high frequency and amplitude impacts.

Observations:

This specimen responded quite well to both heat and vibration excitation, with the heat excitation producing the better result.

The aim of this test was achieved, in that the size of a defect can be determined in the fringe image resulted from ESPI or Shearography test. It can be visually observed that the size of a defect is reflected proportionally in the fringe image. The quantification of the magnitude of the defect itself depends on a number of parameters:

- The amount of excitation energy which is proportional to the number of fringes present in the image.
- Nature and geometry of the defect; it was observed that it is fairly easier to determine the size of a circular defect.

5.3.2 TEST 3: Response of different defects depth location to vibration excitation

The Nomex honeycomb core specimen obtained by sectioning a helicopter rotor blade (fig. 21) was again used for this experiment. This specimen as already indicated, contains 9 circular holes of equal diameter but varying depth as specified in Table. 8. Out of the 9 holes, the three middle ones were selected for testing because they favour the positioning of the vibrator and in the same row there exist a nice spread of defect depth suited for this study (see fig. 28).

Each hole was tested independently; the aim was to determine the frequency, amplitude and time duration required to expose the selected defects depending on the distance from the viewing surface. The panel was placed on the optical table and a Shearography test was conducted. Prior to this, the panel was excited trough vibration, with the vibrator placed at the back of the panel right on the hole undergoing the test.

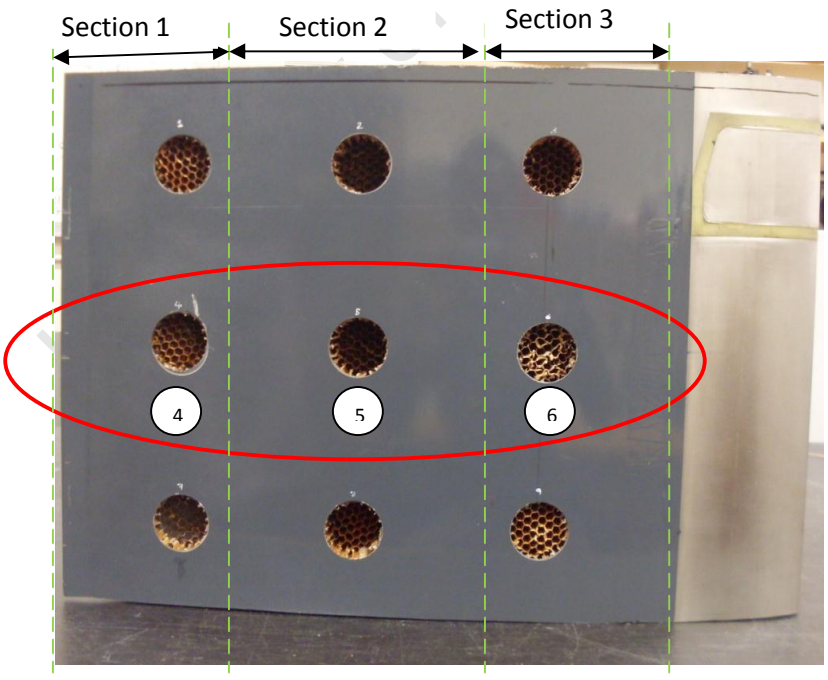

Figure 28: Nomex honeycomb core helicopter rotor blade section with varying depth defects

Table 8: Dimensions for varying depth defects on Nomex honeycomb core specimen (fig. 28)

	Hole no.	section thickness (mm)	Diameter (mm)	Depth (mm)	Distance from end of hole to viewing surface (mm)
Section 1	1	25	45	10	15
	4			20	5
	7			25	0
Section 2	2	53		40	13
	5			40	13
	8			25	28
Section 3	3	70		30	40
	6			10	60
	9			5	65

Once again, checklists were used to mark the combination of frequency and vibration time duration according to the visibility of the defects. This was done individually for each hole as illustrated in Tables. 9, 10 and 11.

Table 9: hole no. 4 (5 mm from viewing surface)

	Time (min)						
Frequency (Hz)	2	5	10	15	20	30	30+
10		✓✓	✓✓✓				
25	✓✓	✓✓✓					
50	✓✓✓						
75							
100							
150							
250							
500							

Table 10: hole no. 5 (13 mm from viewing surface)

Frequency (Hz)	Time (min) 2	5	10	15	20	30	30+
10	✗	✓	✓✓				
25	✓	✓✓	✓✓✓				
50	✓✓	✓✓✓					
75	✓✓						
100	✓✓✓						
150							
250							
500							

Table 11: hole no. 6 (60 mm from viewing surface)

Frequency (Hz)	Time (min) 2	5	10	15	20	30	30+
10	✗	✓✓	✓✓✓				
25	✗	✓✓					
50	✓	✓✓✓					
75	✓✓						
100	✓✓✓						
150							
250							
500							

The circled boxes are the frequency and time combination that exposed the defects fairly well. These have been graphically represented in fig. 29.

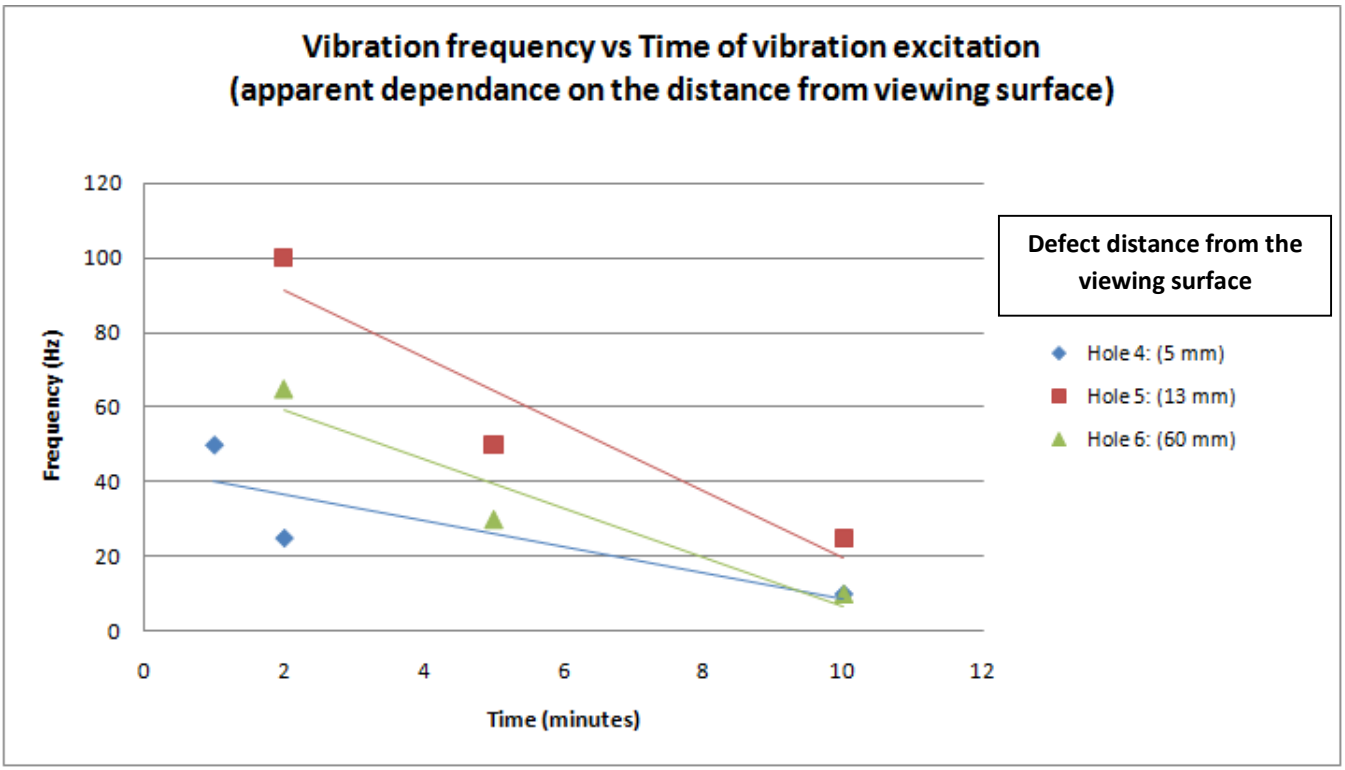

Figure 29: Vibration frequency vs time of vibration excitation apparent dependence on defect depth

As depicted in fig. 29, the frequency/time relationship indicates that the deeper the defect or the closer it is located from the viewing surface, the lesser energy will be required to expose it.

For each frequency and time combination, a certain amount of energy was transmitted through the specimen to expose the defect. This energy will determine how well the defect is revealed. In Table. 12, the fringe images of each hole for the best excitations were collected for illustration purposes.

Table 12: Fringe images of selected holes according to the distance from viewing surface

	Hole no. 4 (distance from S. = 5 mm)			**Hole no. 5 (distance from S. = 13 mm)**			**Hole no. 6 (distance from S. = 60 mm)**		
	Frequency (Hz)								
Time (min)	10	25	50	25	50	100	10	50	100
2			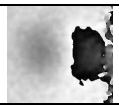			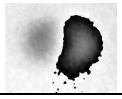			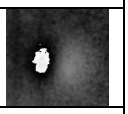
5		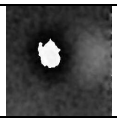						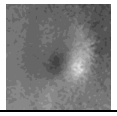	
10	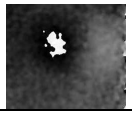			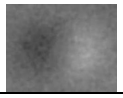			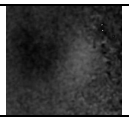		

The more visible fringe images in Table. 12 indicate that more energy was absorbed which occurred at higher frequency. At lower frequencies, even though the amplitude was high, the energy transmitted was not enough to stimulate the defect.

Quantification of the depth of the defect from the fringe image

When applying heat as the excitation method, it is possible to determine the depth of a defect. The number of fringes that appear are dependent on the amount of energy concentrated in the material between the surface and the defect.

For example:

The images in fig. 30 are the fringe patterns of the selected holes in the Nomex honeycomb core from the helicopter rotor blade (fig. 28). These images were taken after the Shearography technique was used with a mild excitation from a lamp as the heat source. The distance between the specimen and the heat source was kept constant and the excitation lasted 0.5 seconds, equally for all holes. This was to ensure that all the holes received the same amount of energy.

As it can be seen from fig. 30, the number of fringes appears to be proportional to the distance of the defect from the viewing surface. The closer the defect is to the viewing surface, the more fringes are present.

In Table 8, the distances from the viewing surface of the selected holes are specified. Hole no. 4 is closer to the viewing surface (5 mm away), and this have been represented in the fringe image by two lobes, with three fringes each. For hole no. 5 which is 13 mm away from the viewing surface, two lobes were presented; the right one with three fringes and the left one with two and a half fringes. Finally hole no. 6, the farthest from the viewing surface (60 mm away) again presented two lobes, each with one and a half fringes. (See Table. 13)

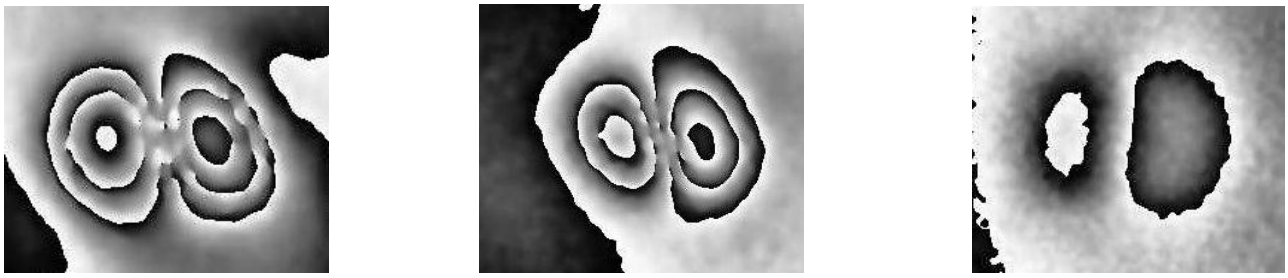

a) Hole no. 4 b) hole no. 5 c) hole no. 6

Figure 30: Fringe images resulted from Shearography tests with heat excitation of the selected holes

Table 13: no. of fringes as an indication of the defect's distance from the viewing surface (images in fig. 30).

	Excitation		Defect		no. of fringe		
Hole no.	method	duration (sec)	diameter (mm)	distance from viewing surface (mm)	Left lobe	Right lobe	Result
4	Applied heat through radiation with a lamp	0.5	45	5	3	3	$\frac{3+3}{2} = 3$
5				13	2.5	3	$\frac{3+2.5}{2} = 2.75$
6				60	1.5	1.5	$\frac{1.5+1.5}{2} = 1.5$

In this example the distance from the viewing surface to a defect is independent from the other defects because they are located in different sections of the panel and the thickness in each section is different from each other (see fig. 28). For this reason, the number of fringes can only be affected by the distance from the viewing surface, or the amount of material between the bottom of the hole and the viewing surface skin.

Figure 31 is the graphical representation of the result from Table. 13, indicating a linear relationship between the number of fringes and the distance of the defect located below the viewing surface.

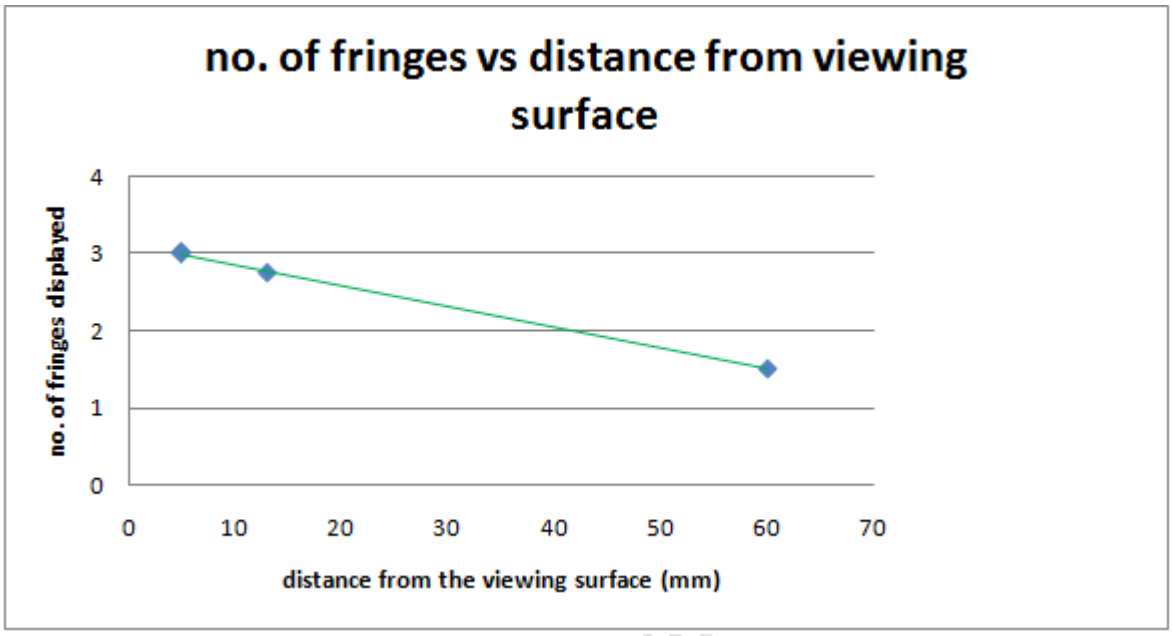

Figure 31: no. of fringes vs position of a defect below the surface

Figure 31 therefore can be interpreted as the ñcalibrationò for the material and the type of flaw. In other words it is a customized solution, only applicable to the described conditions (i.e. material, defect and testing protocol).

Using fig. 31, the position (depth wise) of any other defect in the panel could be approximated from its fringe image. All that will be required is to count the number of fringes exhibited in the fringe pattern and consult the graph to read the corresponding distance from the viewing surface.

The same principle that was used to determine the defectôs distance from the viewing surface using the fringe image, after a mild heating excitation with a lamp, was used to determine the distance of a defect from the viewing surface after vibration excitation.

Unfortunately the fringe image of the defect that emerged after vibration excitation, does not allow for counting fringes vs distance from viewing surface. A probable reason could be that

the vibration energy does not convert into heat energy very efficiently (i.e. it does not get hot enough to cause noticeable surface gradient above the defect).

In fig. 32 the images have been taken individually, with the vibrator placed right on the defect, after 10 minutes of vibration excitation at 100 Hz. There is no pattern in the results presented in fig. 32 that can be used to determine the distance of the defects from the viewing surface.

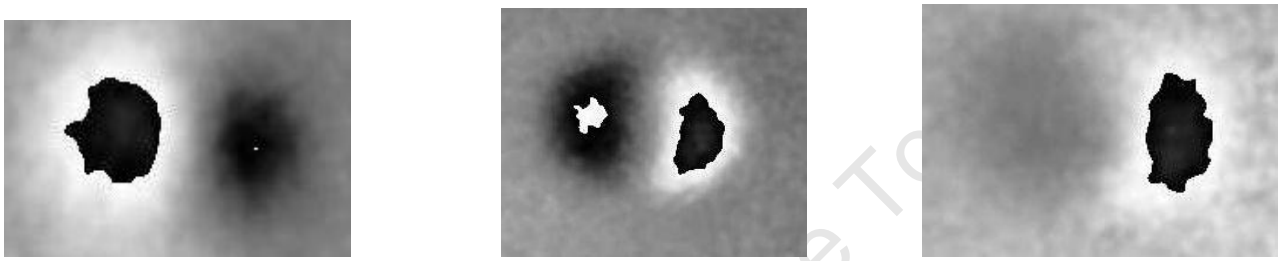

a) hole no. 4 **b) hole no. 5** **c) hole no. 6**

Figure 32: Fringe images resulted from Shearography tests of the selected holes after vibration excitation

5.3.3 TEST 4: Sensitivity of vibration excitation to small deformation

The specimen in fig. 33 is a sandwich composite of GFRP skin and Nomex Honeycomb core. This specimen was cut-out from the wing of an unnamed air vehicle (UAV). The defects induced in this specimen were impacts intended to damage the core but not very visible from the exterior. These defects were induced by applying pressure in the marked areas.

The aim with this specimen was to determine the sensitivity of ESPI and Shearography in conjunction with vibration excitation to small internal deformations caused by suddenly applied external pressure such as impact, shock, etc.

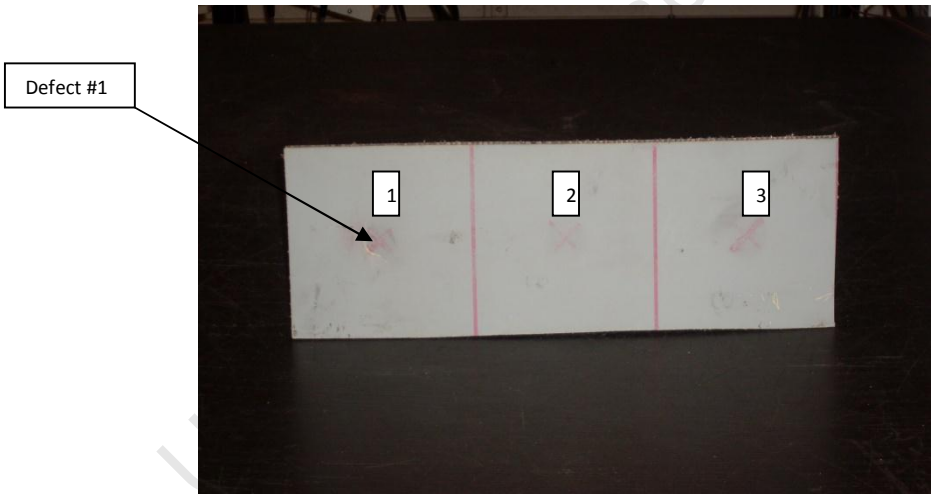

Figure 33: Panel specimen of GFRP skin with Nomex Honeycomb core

This specimen was tested with a frequency of 100 Hz and 5 minutes vibration excitation duration. These parameters have already been determined above for Nomex honeycomb core sandwich composite materials. The fringe images resulted from the ESPI and Shearography tests are presented in fig. 34 and 35.

a) ESPI tests

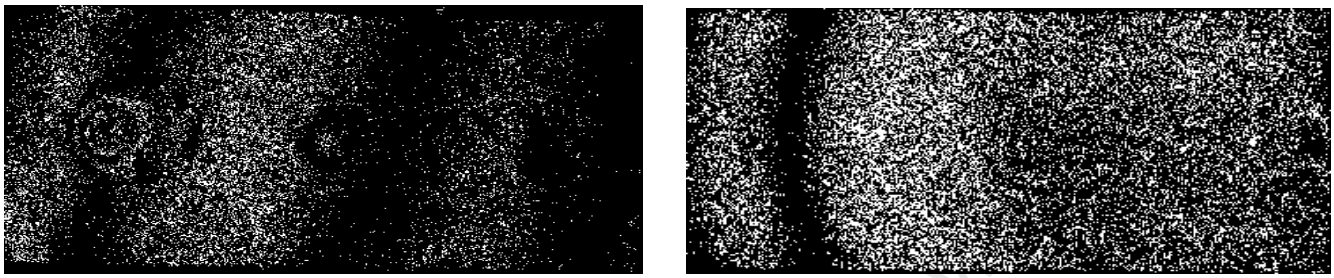

i) ESPI (3 sec heat excitation) ii) ESPI (vibration excitation at 100 Hz & 5 minutes)

Figure 34: Fringe images resulted from ESPI tests of a specimen of GFRP skin and Nomex honeycomb core

b) Shearography tests

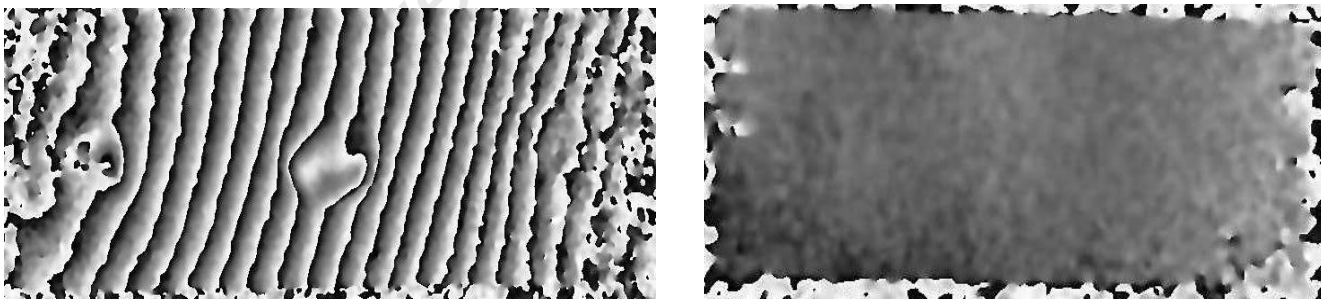

i) Shearography (3 sec heat excitation) & 5 minutes) ii) Shearography (vibration excitation at 100 Hz

Figure 35: Fringe images resulted from Shearography tests of a specimen of GFRP skin and Nomex honeycomb core

Observations:

This test has revealed that both the skin and core must be deformed beyond the elastic limit with possible visible damage before it is detected as a defect with either ESPI or Shearography after vibration excitation. This is probably the reason why defect no. 1, produced by the heaviest impact and slightly visible surface damage is more prominent than the others.

The Nomex Honeycomb core in this specimen was a thin section (3 mm), and probably the vibration response of the GFRP skin had a dominant effect on the overall behavior of the specimen, because GFRP is a viscoelastic material used often for vibration damping and sound control.

The damping property of a material signifies its ability to reduce the transmission of vibration caused by mechanical disturbances. The measure of damping of a material is its damping factor ɖ. A high value of ɖ is desirable for reducing the amplitude of vibration in a structure. Accordingly in fig. 36, CFRP presents higher damping properties than GFRP, but still the damping factor of GFRP is considerably high.

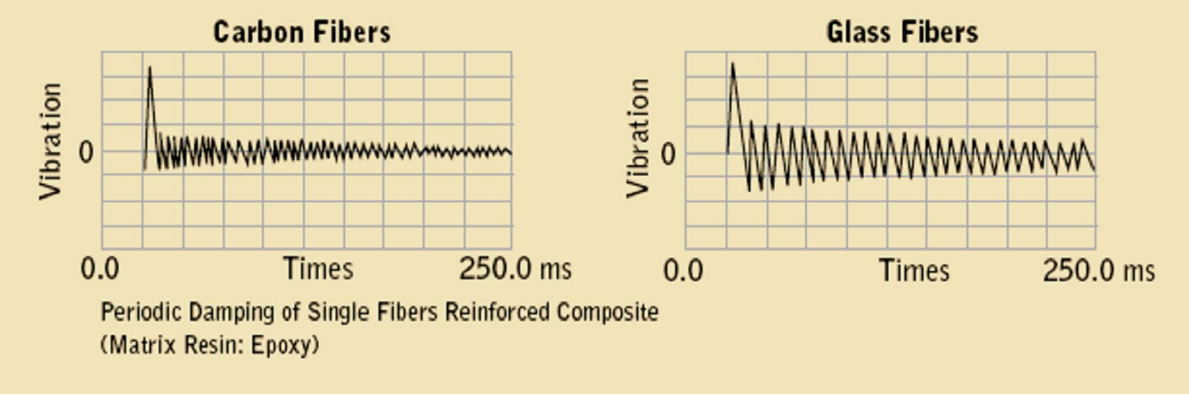

Figure 36: Vibration damping profile of CFRP and GFRP [39]

Another factor that may have contributed for the Nomex Honeycomb sandwich composite with CFRP skin to produce better results than that with GFRP skin is because GFRP exhibits more hysteresis losses than CFRP. Hysteresis losses in ferrous materials come from the molecules in the core laminations resisting being magnetized and demagnetized by the alternating magnetic field. The Greek word, hysteresis, means "to lag" and refers to the fact that the magnetic flux lags behind the magnetic force. In non-ferrous materials such as GF, this happens in a form of delay. This means that the system experiences the effect of the input energy long after it was induced, by the time the material responds, most of the energy has been dissipated. [40]

5.4 Fiber Reinforced Plastic (FRP) composite sandwich with Airex C70.75 core

A number of thermoplastic foams are also used in the aerospace industry as core materials, some of these are commonly known as PVC foams. These materials are available in a wide range to satisfy specific applications in the aerospace industry.

One of the most popular PVC foam core materials used in the aerospace industry is Airex® R82. It is a high performance foam that combines outstanding fire resistance with low smoke and toxicity, along with excellent dielectric properties. It has a high strength to weight ratio, low moisture absorption and it is thermoformable and ductile. It is an exceptional core material for use in the aerospace industry, more specifically in applications that demand structural fire resistance. It is required to be transparent to radar, and operate in extreme hot or cold environments.

Its application in the aircraft and aerospace industry involves: interiors, cockpit doors, cryogenic tanks, insulating panels, radomes, helicopter rotor blades, general aviation fuselage, etc. [36]

Another PVC foam core material that is often used in aerospace industry for similar purposes is the Airex® C70 family. This material has superior mechanical properties than Airex® R82, but the later is better in terms of ductility and transparency.

Airex® R82 PVC foam material was the core material of choice for this project because of its popularity, but because of its unavailability at the time, Airex® C70.75 was used. This material was assembled together as sandwich composite with both CFRP and GFRP as the skin material (fig. 37).

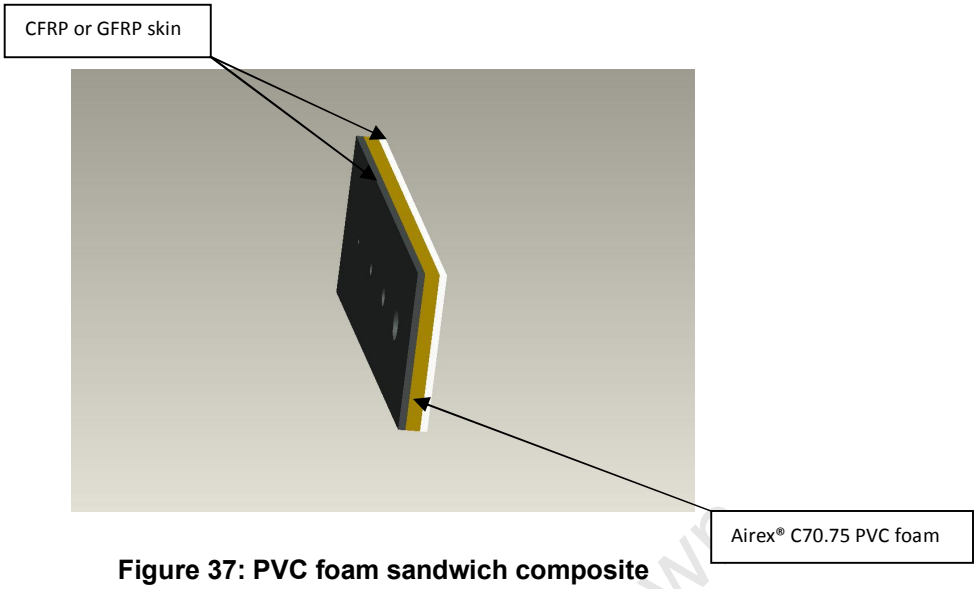

Figure 37: PVC foam sandwich composite

Three specimens were constructed with Airex C70.75 core, two of them with GFRP skin and one with CFRP skin. These specimens were all manufactured in the UCT composites laboratory. The fiber cloths were laid layer by layer while adding the pre-mixed resin. Once the number of layers that amounted to the required skin thickness was laid achieving (2 mm per skin for this project) the core was added and the process was repeated for the top skin. Next, the vacuum bag was prepared over the mixture, to extract the air, get rid of the excess resin and dry the specimen in the process. To achieve the 2 mm thickness, eight layers of carbon fiber cloth were put together for the CFRP skin and six layers of glass fiber cloth were assembled for the GFRP skin.

Care was taken while preparing these specimens so that defects were not introduced in the process. The defects shown below were all introduced after the specimens were constructed.

5.4.1 TEST 5: Testing for different void depth in a specimen of (CFRP) skin and AIREX C70.75 core

The specimen in fig. 38 is a sandwich composite of CFRP skin and AIREX C70.75 core. The defects introduced in this specimen were four circular external voids of diameter 20 mm. The diameter is constant for all four voids but the depth changes from 3 mm for void #1, to 6, 9 and 12 mm for the other voids.

The aim with this specimen was to determine what effect if any the depth of the defect had on the fringe image generated while testing. This was already studied in Test. 3 (page 53), using a Nomex honeycomb core sandwich composite. This test was to determine how the detection of the defects, located at different depth from the viewing surface, was affected by the core material.

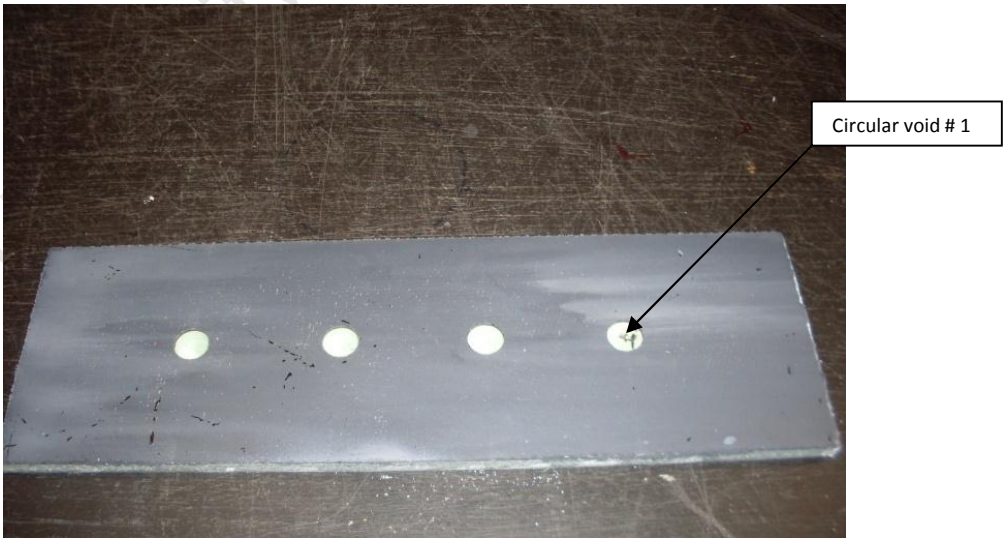

Figure 38: Specimen of CFRP skin and AIREX C70.75 core with external void defects

The same process used in previous tests to determine the frequency and vibration excitation time duration was again followed to determine the frequency and vibration time duration that should be used to excite this specimen and the results for testing void no. 1 of the specimen in fig. 38 are tabulated in Table. 14.

It was already established that more energy is required to make the smallest defect and the defect farthest from the viewing surface of a specimen, visible after vibration excitation. If the entire surface of a specimen is to be excited, the frequency and vibration time duration that makes the smallest defect and the farthest from the viewing surface visible will obviously be the more appropriate one to use. For this reason only the frequencies and vibration time duration that could make void no. 1 of the specimen in fig. 38 visible was assumed good enough to excite the entire specimen.

Table 14: checklist for void no. 1 of specimen in fig. 38 (CFRP skin and AIREX C70.75)

	Time (min)						
Frequency (Hz)	2	5	10	15	20	30	30+
10	✗	✗	✓	✓✓			
25	✗	✓	✓✓				
50	✓	✓✓	✓✓✓				
75	✓✓	✓✓✓					
100	✓✓✓						
150							
250							
500							

Table 15: Frequencies and vibration time duration that made void no. 1 visible

Void no. 1: depth = 3 mm	
Frequency	**Time**
(Hz)	**(min)**
50	10
75	5
100	2

This test proved that not only the proximity from the viewing surface determines the frequency and vibration time duration required to expose a defect in a specimen but also the type of core material.

From Table. 15, 100 Hz and 2 minutes vibration excitation duration was used to excite void no. 1 of the specimen but because the vibration excitation was to cover the entire specimen, 5 minutes vibration duration was used for the excitation of the whole specimen. The resultant fringe images from Shearography and ESPI testing of this specimen after vibration excitation compared to those resulted from heating excitation are presented in fig. 39 and 40.

a) ESPI tests

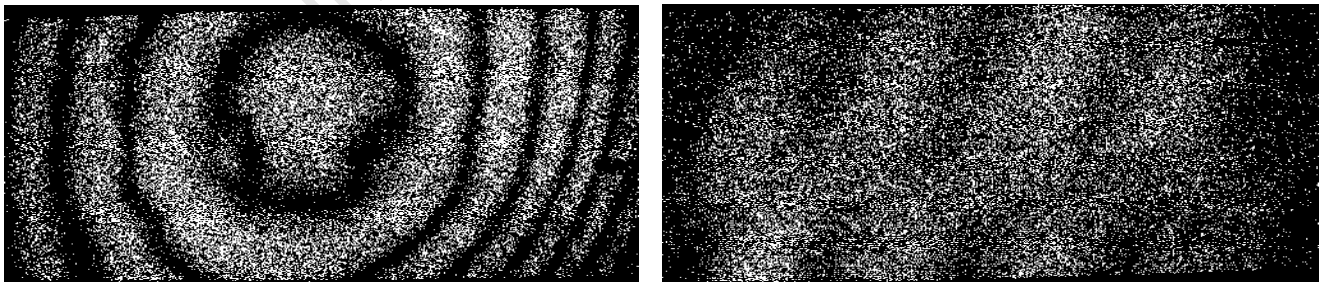

i) ESPI (3 sec heat excitation) **ii) ESPI (vibration excitation at 100 Hz & 5 minutes)**

Figure 39: Fringe images resulted from ESPI tests of the specimen of CFRP skin and AIREX C70.75 core

b) Shearography testing

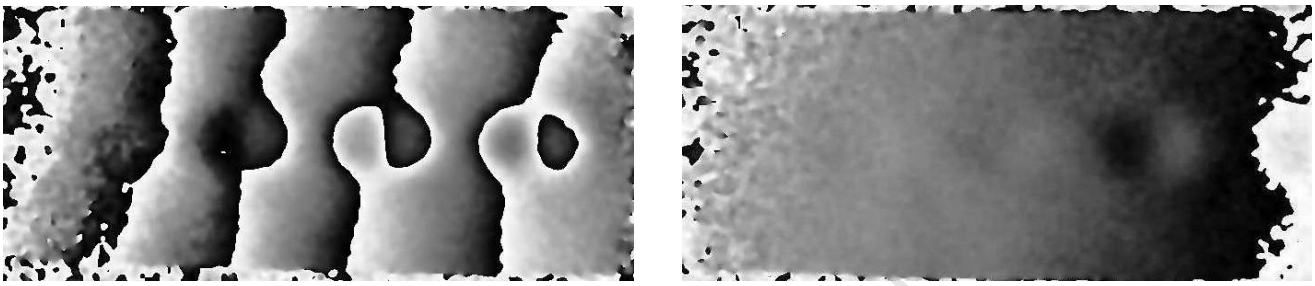

i) Shearography (3 sec heat excitation) and 5 minutes)

ii) Shearography (vibration excitation at 100 Hz

Figure 40: Fringe images resulted from Shearography tests of the specimen of CFRP skin and AIREX C70.75 core

Observations:

With this particular composite it was noticed that just as composite laminates have specific properties determined by the selected reinforcements and matrix resins, sandwich panels take on many additional characteristics that are uniquely determined by the selected core material. PVC foams demonstrate a wide range of elasticity, from blended "cross-linked" foams to "linear" foams, which makes them suitable for vibration damping applications; coupled with the high vibration damping factor of the CFRP skin, made this composite unresponsive to vibration excitation.

5.4.2 TEST 6: Testing internal delaminations and external voids in specimens of GFRP skin and AIREX C70.75 core

The specimen in fig. 41 is a sandwich composite of GFRP skin and AIREX C70.75 core. Four Teflon inserts have been inserted in this specimen as internal defects (delaminations). The diameter of the Teflon inserts varies from 15 mm for the smallest and then 20, 25 and 30 mm for the other defects. These defects were positioned between the core and the skin, at the centerline of the panel 80 mm apart.

The aim of experimenting with this specimen was to establish the smallest delamination detectable.

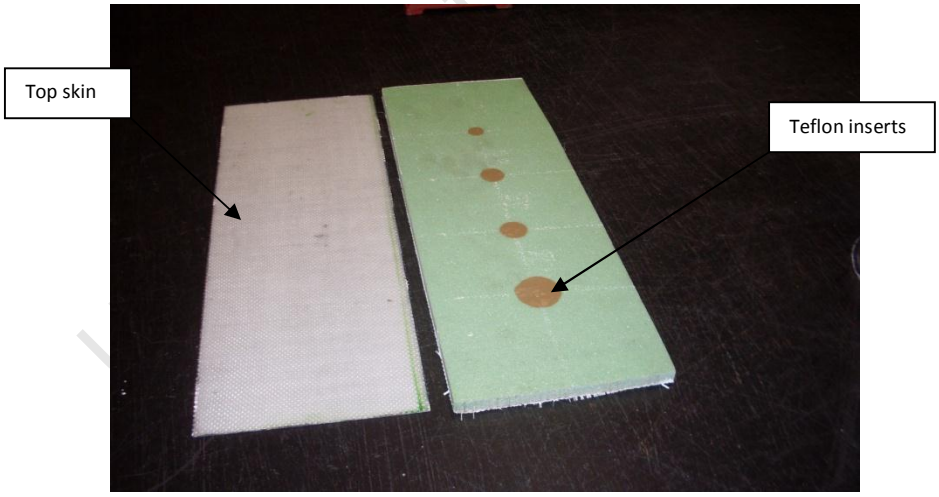

Figure 41: Specimen of GFRP skin and AIREX C70.75 core with internal delaminations of Teflon inserts

The frequency and vibration time duration (100 Hz and 5 minutes) previously used to excite a sandwich composite with AIREX C70.75 core was also used to excite this specimen. The

resultant fringe images from ESPI and Shearography with vibration excitation compared to heating excitation of this specimen are displayed in fig. 42 and 43.

a) ESPI tests

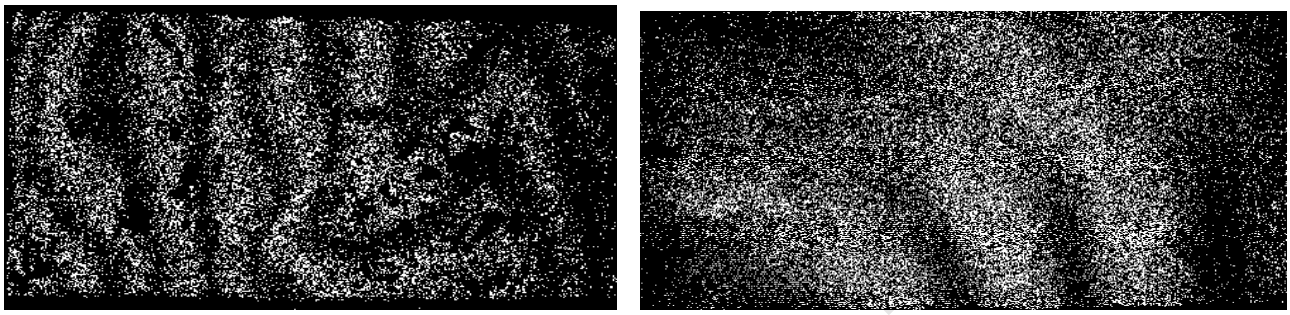

i) ESPI (3 sec heat excitation) ii) ESPI (vibration excitation at 100 Hz and 5 minutes)

Figure 42: Fringe images resulted from ESPI tests of AIREX C70.75 core panel with internal delaminations

b) Shearography tests

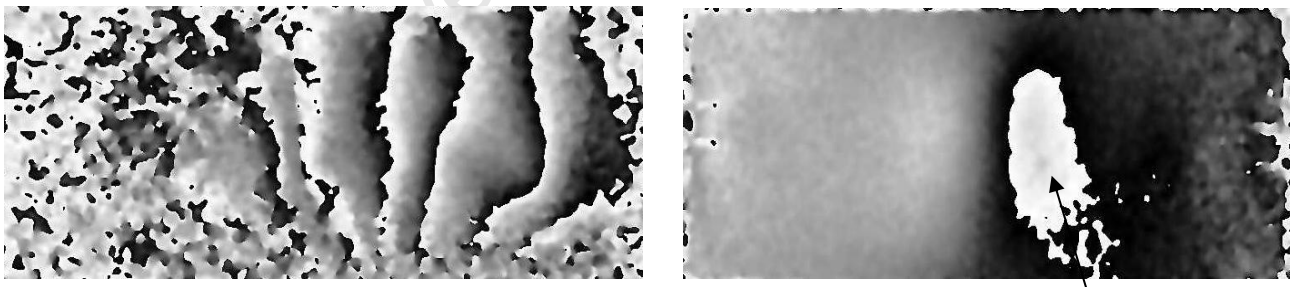

i) Shearography (3 sec heat excitation) and 5 minutes) ii) Shearography (vibration excitation at 100 Hz

Figure 43: Fringe images resulted from Shearography tests of AIREX C70.75 core panel with internal delaminations

The specimen illustrated in (fig. 44) is almost identical as the one in fig. 41; the only difference is that the varying diameter internal defects (delaminations) in the previous specimen are now varying diameter external voids.

The aim when testing this specimen was to determine the minimum detectable void. The voids were machined at a constant depth of 5 mm from the top skin, varying their diameter from 10 mm for the smallest hole to 15, 20 and 25 mm for the others.

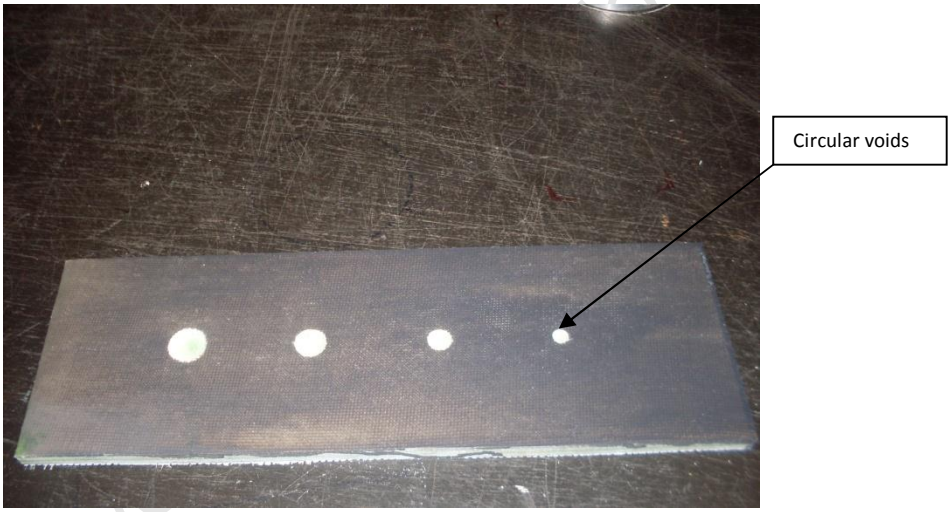

Figure 44: Specimen of GFRP skin and AIREX C70.75 core with external void defects

The same frequency and vibration excitation time duration (100 Hz and 5 minutes) was used to excite this specimen. The fringe images resulted from ESPI and Shearography tests of this specimen are illustrated fig. 45 and 46.

a) ESPI tests

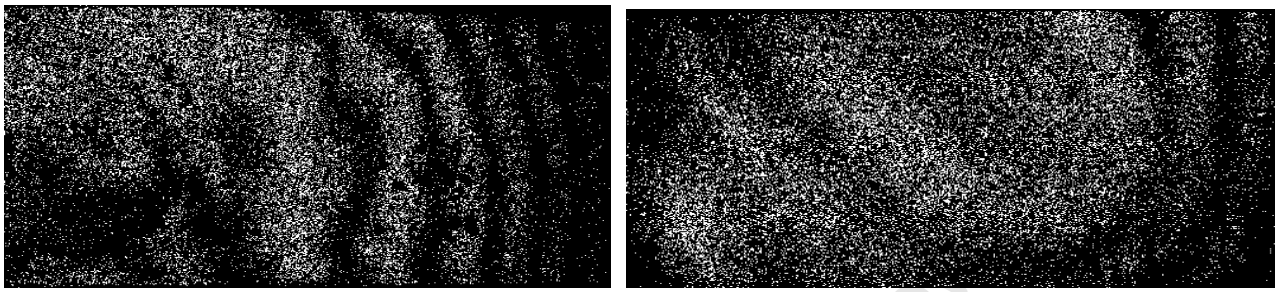

i) ESPI (3 sec heat excitation)

ii) ESPI (vibration excitation at 100 Hz and 5 minutes)

Figure 45: Fringe images resulted from ESPI tests of AIREX C70.75 core panel with external voids

b) Shearography tests

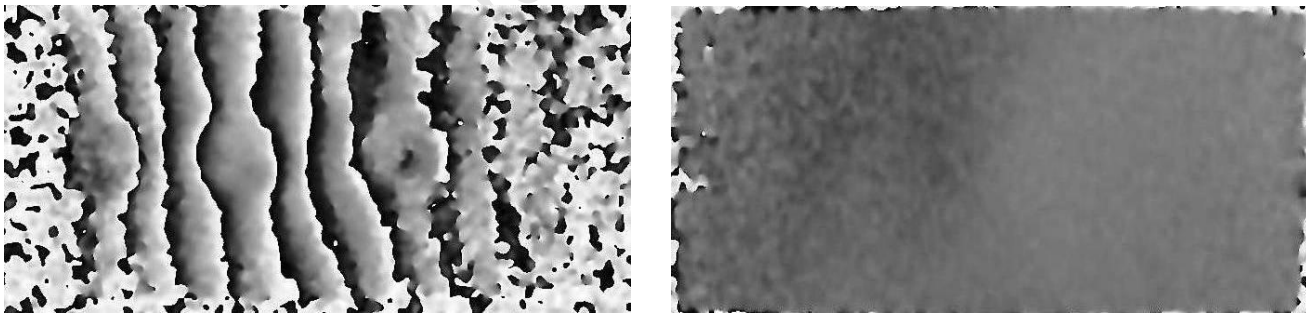

i) Shearography (3 sec heat excitation)

ii) Shearography (vibration excitation at 100 Hz and 5 minutes)

Figure 46: Fringe images resulted from Shearography tests of AIREX C70.75 core panel with external voids

Observations:

Very poor results were obtained with the GFRP skin specimens, especially those from vibration excitation. For this reason, the smallest detectable void and delamination could not be determined with these specimens.

The constituent or primary composite materials of the above sandwich specimens were PVC foam as the core material and the skin was GFRP. The skin and core are both high vibration damping materials, coupled with the hysteresis losses of the GFRP was enough to prevent the transmission of any significant amount of vibration energy to expose the flaws.

The principle with vibration excitation is to generate heat in the material, achieved from the friction between the defect surfaces. The specimen that contained internal defects of Teflon inserts between the core and the upper skin possibly did not experience any friction. During the vibration excitation period, there was probably very little rubbing in the location of the defects to generate some localized heat. Teflon itself is a low modulus material that could very well act as vibration damper and its smoothness could possibly act as a lubricant.

The defects in the second specimen being external voids, did not allow for rubbing to take place and generate some localized heat.

5.5 Perspex/Polycarbonate

Perspex is a premium grade of acrylic sheet, one of the thermoplastics often used in the aerospace industry. This material is preferred above others in specialized applications because of its moderate properties, which includes excellent optical clarity and light transmission properties. One of the downsides of this material is that it is brittle when loaded.

Polycarbonates in the other hand, is a particular group of thermoplastic polymers with similar properties to Perspex and good flexural strength.

The original application of Perspex/Polycarbonates in aerospace industry was as a glazing component in military and civil aircraft. Currently, they are commonly used as the material of choice for aircraft windscreens, aircraft canopies, tray tables and even for seals and bearings. [38]

Perspex was chosen to construct laminate specimens with internal delaminations, with Polycarbonate as a substitute because of commercial availability.

Two specimens were constructed for testing using Polycarbonate. One of the specimens contained defects at different depths and the other contained different size defects (fig. 47 and 53).

5.5.1 TEST 7: Testing internal delaminations in Polycarbonate laminate composite

The specimen manufactured for this experiment is displayed in fig. 47. This specimen was constructed by gluing three polycarbonate sheets together with chloroform and inserting three equally spaced squares Teflon inserts size 20 x 20 mm between two sheets. The thickness of each sheet is 2 mm. The squares were first machined to 0.2 mm depth in one sheet before inserting the Teflon. The three sheets were put together so that the testing could be conducted with the defects at different depth depending on the selected viewing face; when viewed from one face the depth will be the thickness of one sheet (2 mm) and when viewed from the other face, the depth will be the thickness of two sheets (4 mm).

The transparency of this specimen resulted in a very weak object light reflection beam which could not be read effectively by the CCD camera. This problem was resolved by coating the specimen with mat white spray paint.

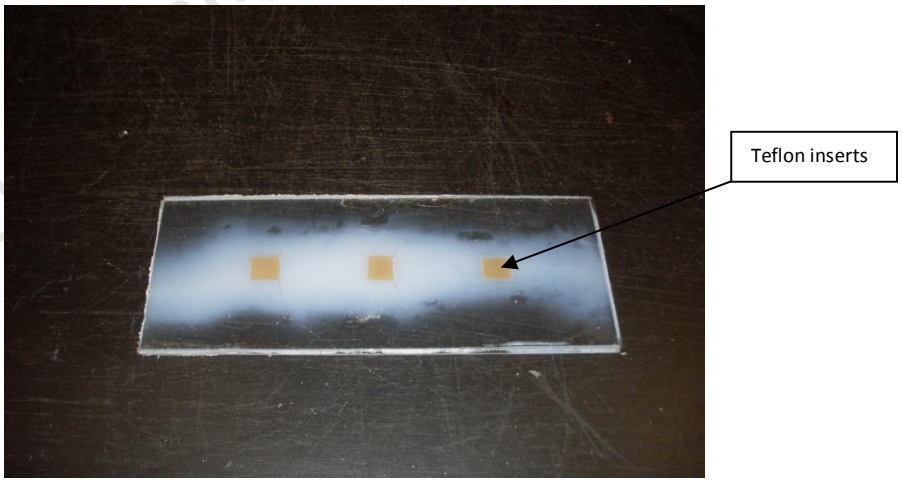

Figure 47: Polycarbonate specimen with internal delaminations of Teflon inserts

Figure 48: Polycarbonate specimen after spray painting

The frequency and vibration time duration were also determined for this specimen. Because of the relative ductility of this material, the frequency and amplitude was kept at a moderate level to prevent damaging it. For this reason in this test, instead of constantly increasing the frequency till the defect was visible, the vibration excitation duration was increased. The checklist used to select the frequency and vibration duration is displayed in Table. 16.

Table 16: Checklist for Polycarbonate specimen

	Time (min)						
Frequency (Hz)	2	5	10	15	20	30	30+
10	✗	✓	✓✓	✓✓✓			
25	✓	✓✓	✓✓✓				
50	✓✓	✓✓✓					
75							
100							
150							
250							
500							

The above checklist was obtained with the vibrator placed on the centre defect (delamination) in the specimen in fig. 47. The frequency and vibration time duration that best revealed the defect in this specimen are tabulated in Table. 17.

Table 17: Frequency and vibration time duration best revealed the defect in Polycarbonate

Frequency (Hz)	Time (min)
10	15
25	10
50	5

The resultant fringe images from the Shearography and ESPI testing of this specimen after vibration excitation compared to those resulted from heating excitation are presented in fig. 49 to 50.

a) ESPI tests

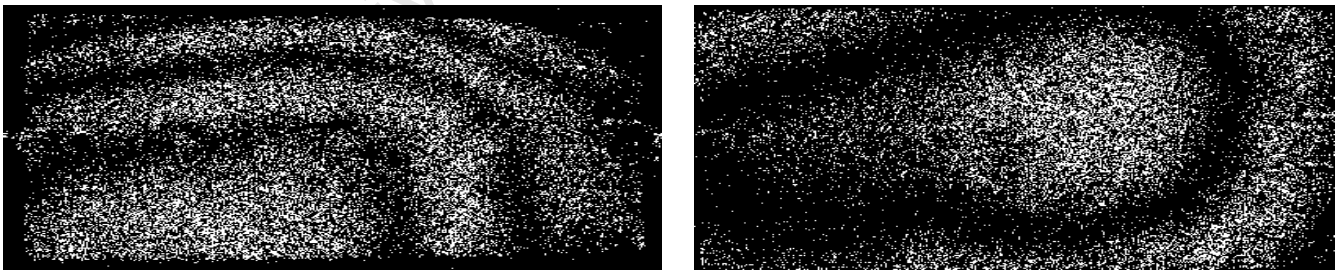

i) ESPI face1: 2 mm depth (3 sec heat excitation) ii) ESPI face1: 2mm depth (vibration excitation at 50 Hz & 5 minutes)

Figure 49: Fringe image resulted from ESPI test of Polycarbonate specimen with internal delaminations at 2mm depth

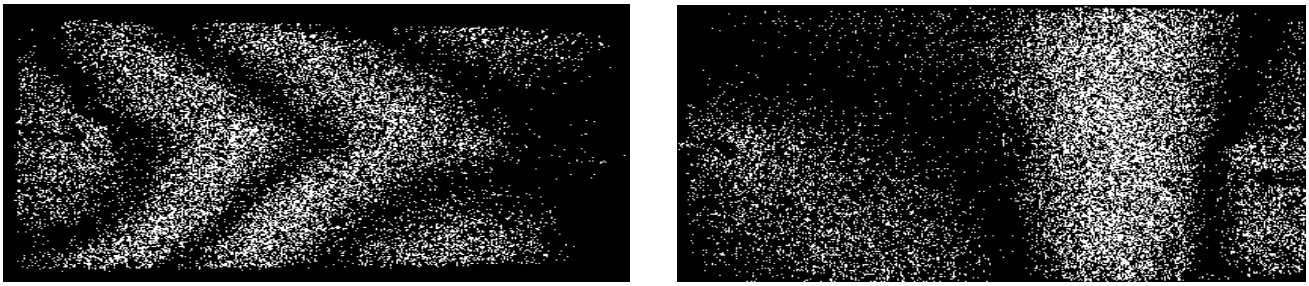

i) ESPI face2: 4 mm depth (3 sec heat) ii) ESPI face2: 4mm depth (vibration at 50 Hz & 5 minutes)

Figure 50: Fringe image resulted from ESPI test of Polycarbonate specimen with internal delaminations at 4 mm depth

b) Shearography tests

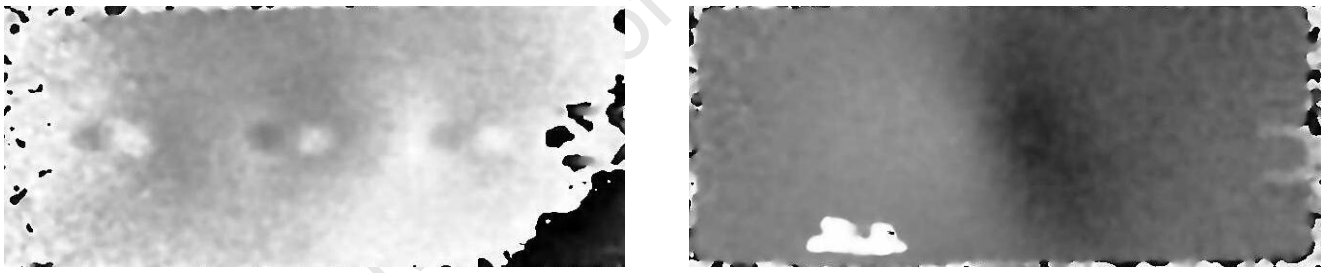

i) Shearography face1: 2 mm depth (3 sec heat) ii) Shearography face1: 2mm depth (vibration at 50 Hz & 5 minutes)

Figure 51: Fringe image resulted from Shearography test of Polycarbonate specimen with internal delaminations at 2mm depth

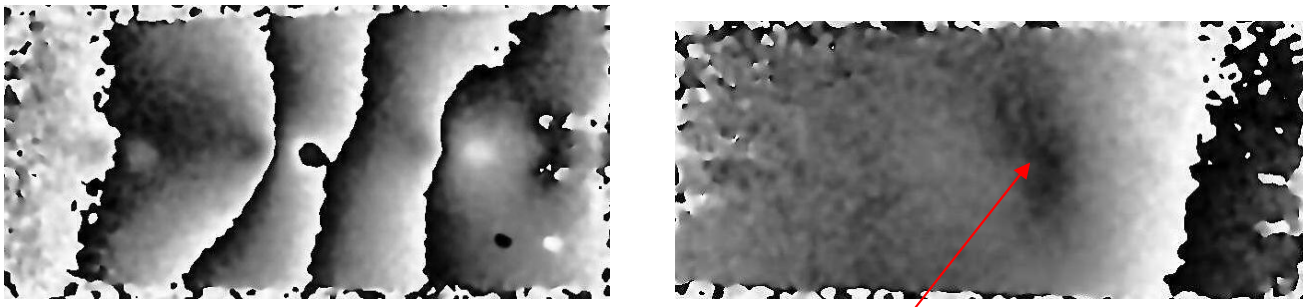

i) Shearography face1: 2 mm depth (3 sec heat) **ii) Shearography face1: 2mm depth (vibration at 50 Hz & 5 minutes)**

Figure 52: Fringe image resulted from Shearography test of Polycarbonate specimen with internal delaminations at 4 mm depth

The detection of different size defects in the Polycarbonate specimen was accomplished by a specimen that was constructed as seen in fig. 53, and then coated with white spray paint. The defects sizes were 10 x 10 mm, 20 x 20 mm and 30 x 30 mm.

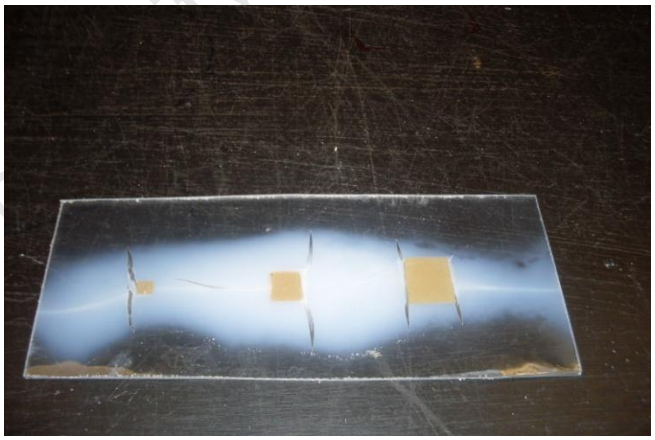

Figure 53: Polycarbonate specimen with internal Teflon inserts of different sizes

The frequency of 50 Hz and vibration time duration of 5 minutes that was chosen to excite the previous Polycarbonate specimen was also used in this one. The resultant fringe images from the Shearography and ESPI testing with vibration excitation compared to those resulted from heating excitation are presented in fig. 54 and 55.

a) ESPI tests

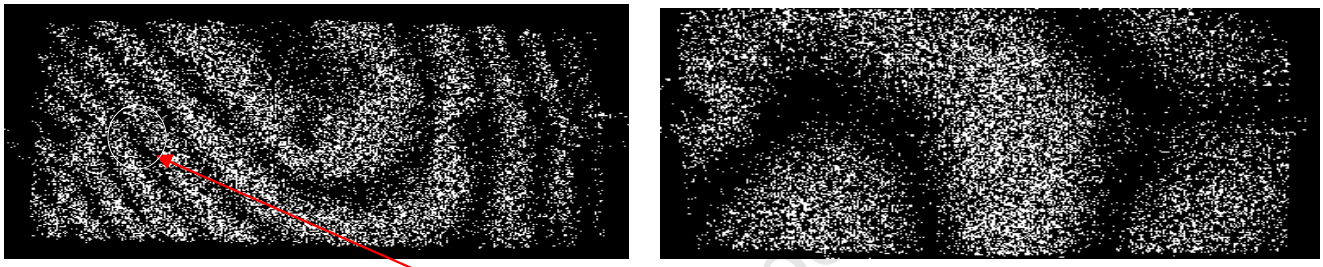

i) ESPI (3 sec heat excitation) and 5 minutes)

ii) ESPI (vibration excitation at 50 Hz

Figure 54: Fringe images resulted from ESPI test of Polycarbonates specimen with different size delaminations

b) Shearography tests

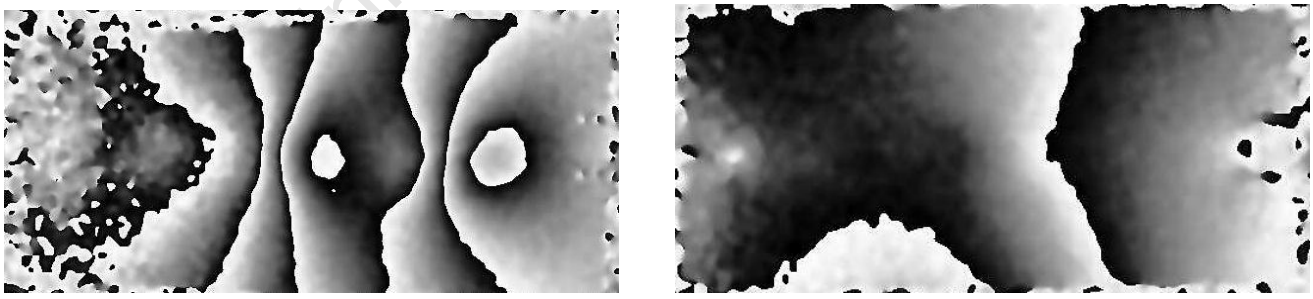

i) Shearography (3 sec heat)

ii) Shearography (vibration at 50 Hz and 5 minutes)

Figure 55: Fringe images resulted from Shearography test of Polycarbonates specimen with different size delaminations

Observations:

It was again observed that vibration excitation was not suitable to excite low modulus materials for NDT with ESPI or Shearography. In this particular example the specimen was polycarbonate, a thermoplastic polymer, and it is here confirmed that the viscoelastic properties of polymers give them the unique ability to be used as effective vibration damping materials. Furthermore it appears that ESPI testing did not yield any ólikeò results when compared with the visibility of the defects shown in the Shearography tests.

Finally, in some of the fringe images, a hot spot shows only in the point of contact, where knocking took place with the vibrator to transmit vibrational energy into the specimen.

CHAPTER 6: CONCLUSIONS

This study was conducted in order to determine the suitability of using vibration excitation for the NDT of composites in detecting delaminations and debonds using ESPI and Shearography techniques. The scope of the project focused only on fibre reinforced composites (FRC) in either laminated or sandwich composition commonly used in the aerospace industry. Several specimens were constructed from different FRCs and different geometry defects were introduced in the specimens with the aim of establishing the detectability of these defects.

Although it was known in advance that the materials utilized for the specimens hold properties such as vibration damping, thermal insulation and hysteresis, the tests needed to be conducted in order to ascertain the extent to which these properties would inhibit the detection of defects such as delaminations and voids, when the specimens containing these defects were excited by vibration.

The result from the tests revealed that vibration excitation was not the appropriate method to excite FRCs for defect detection using ESPI or Shearography, due to the following:

1. **Vibration damping;** most of the structural composite materials used in the aerospace industry possess vibration damping characteristics. This is particularly desirable for noise absorption and to reduce vibration. It appears that the detection of defects in these materials under NDT with ESPI or Shearography using vibration excitation is severely inhibited, because damping restricts the transmission of vibration energy.

2. **Hysteresis losses;** some composites such as glass fiber, exhibit ñhysteresisòlosses. This causes the molecules in the core to resist being elastically deformed under dynamic loading. This resistance possibly results in no heat generation by friction, because of the lag in response of the material to the input energy. Even though a lot of time was allowed for the vibration excitation, apparently little or no heat was generated

in some of the specimens, thus inhibiting surface thermal strains from revealing the defects underneath.

3. **Thermal insulators;** to minimize the dispersion of fire in the case of an accident and to prevent heat loss, say in the cabin of an aircraft, most of the structural materials used in the aerospace industry are required to be thermal insulators. Some of these materials are more heat resistant than others. This is the reason why some specimens did not respond as well to the heat excitation.

It is suggested here that the properties as described above render the composites immune or non-responsive to the vibration excitation, and in some instances even to thermal excitation. It is evident that vibration as an excitation technique for NDT with ESPI and Shearography for composite materials such as Polycarbonate or CFRP and GFRP with low modulus core (i.e. PVC) is not recommended.

REFERENCES:

1. http:// ma3naido.blogspot.com/2009/10/composite-construction-Aircraft
2. www.environmentalgraffiti.com/.../ Thu, Jul 16, 2009
3. www.gizmag.com/tag/awards
4. www.aviation-history.com/theory/composite.jpg August 2, 2009
5. Praveengouda Patil. A seminar on: Laminated Composites. University Visvesvaraya College of Engineering
6. P.K. Mallick. 1997. Composite Engineering Handbook. University of Michigan-Dearborn. Marcel Dekker, Inc.
7. Pak de Jongko. Bonding of Composite Materials. Duraposita Chem.
8. Mital, Subodh K.; and Murthy, Pappu L.N.: Quantifying Uncertainties in the Thermo-Mechanical Properties of Particulate Reinforced Composites. J. Reinf. Plast. Comp., vol. 19, no. 8, 2000, pp. 657-678.
9. http://www.tms.org/pubs/journals/JOM/0104/Rawal-0104.html: MMCs for Space: Overview
10. www.trl.com/services/materialstesting/mmc_met
11. www.grc.nasa.gov
12. www.mrl.columbia.edu/.../ch05/html/l1c05s03.html
13. www.advanced-materials.at/products/products_A
14. www.ultramet.com/ceramic_matrix_composites_ma
15. www.ihs.com. Adam Quilte. Composite in Aerospace Application
16. http://www.engineersparadise.com/en/ipar/18832

17. http://www.composites.com/images/panels/pic_butfly.gif

18. L. Ko. William. 1979. Supperplastically Formed Diffusion Bonded Metallic Structure. Lancster, California. USA

19. Authors.library.caltech.edu: Tim Palucka and Bernadette Bensaude-Vincent: Composites Overview

20. Gary Savege. 2006. Failure Prevention in Bonded Joints on Primary Load Bearing Structures. BAR Honda Formula 1 Racing Team, Operations Centre, Brackley, Northants NN13 7BD, UK.

21. http://handle.dtic.mil/100.2/ADA263503 ADVISORY GROUP FOR AEROSPACE RESEARCH AND DEVELOPMENT NEUILLY-SUR-SEINE (FRANCE)

22. J. Muric-Nesic, P. Compston, N. Noble, Z.H. Stachurski. 2008. Effect of low frequency vibrations on void content in composite materials. Department of Engineering, College of Engineering & Computer Science, The Australian National University, Canberra, ACT 0200, Australia. Elsevier

23. Peter A. Zinoviev, Yury N. Ermakov.1994. Energy Dissipation in Composite Materials. Technomic Publishing Company, Inc. USA

24. Monoach, E. Trendafilova, I. 2008. Large Amplitude Vibration and Damage Detection of Rectangular Plates. Elsvier ltd.

25. C.M. Vest. 1979. Holographic Interferometry. John Wiley & Sons, Inc.

26. S. Magnussen.2004. Holographic Interferometry and its application in visualizing particle movements in continuous flow. University of Bergen. Norway. Thesis

27. D. Findeis, J. Gryzagoridis. 2004. Portable Shearography and Portable Electronic Speckle Pattern Interferometry: A Presentation of their capabilities

28. H. Gerhard, G. Busse. 2006. Lockin-ESPI interferometric imaging for remote non-destructive testing. Institute for Polymer Testing and Polymer Science (IKP), Department of Non-Destructive Testing, Stuttgart University. Germany. Elsevier Ltd.

29. D. Findeis, J. Gryzagoridis, R.B. Tait.2004. Residual Stress Determination and Defect Detection Using Electronic Speckle Pattern Interferometry.

30. D. Findeis, J. Gryzagoridis and W. Bopape. 2005. Impact Damage Detection on Composites Using Electronic Speckle Pattern Interferometry

31. David, C. Jiles. 2008. Introduction to the Principles of Materials Evaluation. Wolfson Centre for Magnetics. Institute for Advanced Materials and Energy Systems, Cardiff University, UK. Tailor & Francis group.

32. Roger M Groves, Stephen W James and Ralph P Tatam. 2000. Polarization-multiplexed and phase-stepped fibre optic shearography using laser wavelength modulation. School of Mechanical Engineering, Cranfield University, UK.

33. Avinash, A. 2005. A Novel Compact Shearographic NDT System. University of Cape Town, Masters Thesis.

34. www.compositesworld.com/articles/inside-rampd

35. http://www.plascore.com/aerospace-aramid-fiber-honeycomb.htm

36. http://www.amtcomposites.co.za/ac_airexpvcfoams.html

37. M.R. Naniwadekar, S.S. Naik, S.K. Maiti. 2007. On prediction of crack in different orientations in pipe using frequency based approach. Department of Mechanical Engineering, Indian Institute of Technology Bombay, India. Elsevier Ltd.

38. http://www.curbellplastics.com/markets/

39. Vectran. 1999. Grasp The World of Tomorrow, Engineering Data. Celanese Acetate LLC. Charlotte, North Carolina, USA.

40. S. Senthilvelan, R. Gnanamoorthy. 2005. Damping characteristics of unreinforced, glass and carbon fiber reinforced nylon 6/6 spur gears. Department of Mechanical Engineering, Indian Institute of Technology Madras. India